Implementation and application of Ensemble Optimal Interpolation on an operational chemistry weather model for improving $PM_{2.5}$ and visibility predictions

Siting Li[1], Ping Wang[1], Hong Wang[1], Yue Peng[1], Zhaodong Liu[1], Wenjie Zhang[1], Hongli Liu[1], Yaqiang Wang[1], Huizheng Che[1], Xiaoye Zhang[1]

[1]State Key Laboratory of Severe Weather & Key Laboratory of Atmospheric Chemistry of CMA, Chinese Academy of Meteorological Sciences, Beijing, China

Correspondence to: Ping Wang (wangp@cma.gov.cn); Hong Wang (wangh@cma.gov.cn)

Abstract. The data assimilation technique is one of the important ways to reduce the uncertainty of atmospheric chemistry model input and improve the model forecast accuracy. In this paper, an ensemble optimal interpolation assimilation (EnOI) system for a regional online chemical weather numerical forecasting system (GRAPES_Meso5.1/CUACE) is developed for operational use and efficient updating of the initial fields of chemical components. A heavy haze episode in eastern China was selected, and the key factors affecting the EnOI, such as localization length-scale, ensemble size, and assimilation moment, were calibrated by sensitivity experiments. The impacts of assimilating ground-based $PM_{2.5}$ observations on the model chemical initial field and $PM_{2.5}$, visibility forecasts were investigated. The results show that assimilation of $PM_{2.5}$ reduces the uncertainty of the initial $PM_{2.5}$ field considerably. Using only 50% observations to do the assimilation, the root mean square error (RMSE) of initial $PM_{2.5}$ for independent verification sites in mainland China decreases from 73.7 to 46.4 μg m^{-3}, and the correlation coefficient increases from 0.58 to 0.84. An even larger improvement appears in North China. For the forecast fields, assimilation of $PM_{2.5}$ improves $PM_{2.5}$ and visibility forecasts throughout the time window of 24 h. The $PM_{2.5}$ RMSE can be reduced by 10%-21% within 24 h, and the assimilation effect is most remarkable in the first 12 h. Within the same assimilation time, the assimilation efficiency varies with the discrepancy between model forecasts and observations at the moment of assimilation, and the larger the deviation, the higher the efficiency. The assimilation of $PM_{2.5}$ further contributes improvement of visibility forecast. When the $PM_{2.5}$ increment is negative, it corresponds to an increase in visibility, and when the $PM_{2.5}$ analysis increment is positive, visibility decreases. It is worth noting that the improvement of visibility forecasting by assimilating $PM_{2.5}$ is more obvious in the light pollution period than in the heavy pollution period, since visibility is much more affected by humidity during the heavy pollution period accompanied by low or extreme low visibility. To get further visibility improvement, especially for extreme low visibility during severe haze pollution, not only $PM_{2.5}$ but also relative humidity should be simultaneously assimilated as well. The results of this study shows that the EnOI may provide a practical and cost-effective alternative to the EnKF for the applications where computational cost is a main limiting factor, especially for real-time operational forecast.

1 Introduction

Air pollution is an intractable problem that all developing countries with high population in the world are facing at present. $PM_{2.5}$ plays an important role in air pollution, and its concentration will directly affect air quality. From the health perspective, long-term exposure to high concentrations of $PM_{2.5}$ has adverse effects on the human body, including the respiratory system, cardiovascular disease and other chronic diseases(Ghorani-Azam et al., 2016). From the meteorological perspective, aerosol particles can effectively absorb and scatter solar radiation, change the intensity and direction of sunlight, reduce atmospheric horizontal visibility(Liu et al., 2019; Yadav et al., 2022; Ting et al., 2022), leading to haze episodes which are characterized by significant growth in the concentration of aerosol particles and sharp reduction of visibility.

Accurate $PM_{2.5}$ and visibility forecasts are critical for human health, air quality assessment and public transportation safety issues(Zhang et al., 2013). Chemistry Transport Model (CTM) or Coupled chemistry meteorology models (CCMM) are important tools for $PM_{2.5}$ and visibility forecasting, and is pivotal in air quality and atmospheric chemistry research. However, various uncertainties exist in the simulation of atmospheric components in CTM or CCMM, especially for aerosols (Lee et al., 2016). The complexity of atmospheric pollution formation mechanisms and model structure, the uncertainty of chemical initial conditions (ICs) and the lag in emission inventories lead to a deviation of air quality forecast results from observed comparisons. Data assimilation (DA) is one of the most effective ways to improve model predictions. Weather prediction had relied on data assimilation for many decades (Kalnay, 2003; Navon 2009). In comparison, the use of data assimilation in atmospheric chemistry models to improve air quality forecasting is more recent, but important advances have been made. Tombette et al. (2009) presented an experiment on PM_{10} data assimilation using OI method to improve PM_{10} forecasting. Tang et al. (2015) used the same DA method to assimilate ozone/ $PM_{2.5}$ and MODIS aerosol optical depth data into the Community Multi-scale Air Quality model to improve the ozone and total aerosol concentration for the CMAQ simulation over the contiguous United States. Liu et al. (2011) assimilated AOD from Terra and Aqua satellites using the GSI 3D-Var assimilation system, showing that AOD data assimilation system can serve as a tool to improve simulations of dust storms. Li et al. (2013) and Feng et al. (2018) assimilated ground-based observations of $PM_{2.5}$ using 3D-Var to improve $PM_{2.5}$ forecasting. 4D-Var has been successfully implemented on CTMs and has improved the $PM_{2.5}$ forecasting capability. Zhang et al. (2016) constructed a GEOS-Chem adjoint model suitable for $PM_{2.5}$ pollution diffusion based on 4DVAR algorithm, which was verified by the monitoring data of APEC in Beijing in 2014. Zhang et al. (2021) built a $PM_{2.5}$ data assimilation system based on the 4DVar algorithm and the WRF-CMAQ model, which can assimilate synchronous observations simultaneously to improve aerosol prediction accuracy. Wang et al. (2021) established a 4D-VAR assimilation system based on GRAPES_CUACE to optimize black carbon (BC) daily emissions in northern China on 4 July 2016. EnKF also plays a significant role in improving the accuracy of atmospheric chemistry model forecasts. Lin et al. (2007) developed a EnKF system for a regional dust transport model. Tang et al. (2016) investigated a cross-variable ozone DA method based on an EnKF, for improving ozone forecasts over Beijing and surrounding areas. Park et al. (2022) developed a DA system for the CTM using the EnKF technique, where $PM_{2.5}$ observations from ground stations are assimilated to ICs every 6 hours to improve $PM_{2.5}$ forecasting in the Korean region.

Peng et al. (2017) used EnKF to optimize ICs and emission input, resulting in significant improvements in $PM_{2.5}$ forecast. Overviews of these achievements were provided in several literatures (Bocquet et al., 2015; Benedetti et al., 2018; Zhu et al., 2018; Sokhi et al., 2022).

Although the previous studies have reported DA method using ground-based or satellite-retrieved observation led to improvement of atmospheric composition prediction, each of these DA methods has its own limitation. In OI and 3D-Var, the background error covariance (BEC) matrix is estimated at once and the prediction error is statistically stationary. 4D-Var and EnKF are advanced data assimilation methods that provide the evolution of the forecast error covariance, but when they are employed in the operation use, each of them is facing their own challenge. The CTM and CCMM are complex systems with rapid updates, and the implementation of 4D-Var requires a large workload of adjoint models coding (Ha, 2022). EnKF obtains a flow-dependent BEC using ensemble forecast by integrating the model multiple times, and that makes it approximately 100 times more computationally expensive than the forward model when applied to nonlinear systems (Counillon and Bertino, 2009). Compared to EnKF, EnOI is a suboptimal method for ensemble-based assimilation (Evensen, 2003). EnOI uses a stationary ensemble to estimate the BEC and only one analysis field is updated at a time, which makes the computation time greatly reduced. EnOI can be used in conjunction with other DA methods and may be an appropriate choice for coupled forecast systems(Oke et al., 2010). EnOI has been widely used in ocean models with significant improvements to model forecast (Counillon and Bertino, 2016; Castruccio et al., 2020; Xie and Zhu, 2010; Belyaev et al., 2021), but not in the CTM or CCMM. To our knowledge, there are only several papers involved researches of EnOI in atmospheric chemistry models so far. Zhang et al. (2014) implement the EnOI on an air quality numerical modelling MM5-STEM for the Pearl River Delta region in China. They found that EnOI produced the initial condition closer to the true situation, but they didn't investigate the effect of EnOI on forecast. Wang et al. (2016) used EnOI to investigate the possibility of optimally recovering the spatially resolved emissions bias of black carbon aerosol. Kong et al. (2021) applied EnOI to assimilate hourly surface observations of CO concentrations at 1107 sites over China in January 2015. They found that simulations with the updated emissions revealed a decrease bias of average CO concentrations at 349 independent validation sites from 0.74 mg m^{-3} to 0.01 mg m^{-3} and a reduction of the RMSE by 18%. Results from these papers showed that EnOI is a useful and computation-free method to reduce the errors of initial chemical condition or emissions. Since development of CCMM are fairly recent, EnOI have not applied for real-time CCMM yet. The GRAPES-CUACE is an online CCMM system developed by the China Meteorological Administration (Gong and Zhang, 2008; Zhou et al., 2008; Wang et al., 2010a). This model not only plays an important role in the scientific research on air pollution (Wang et al., 2015a; Wang et al., 2015b), aerosol-cloud interaction (Wang et al., 2018; Peng et al., 2022); and aerosols' weather feedback (Wang et al., 2010b; Zhang et al., 2022), but is also applied for the operational forecasting of air quality, Fog-Haze weather and dust storm in China (Wang and Niu, 2013; Liu et al., 2017). Very recently, this model system has been updated to a new version (GRAPES_Meso5.1/CUACE) with many improvements (Wang et al., 2022). In this study, we established a real-time EnOI chemistry initial fields $PM_{2.5}$ assimilation system for this new version of model, with assimilating $PM_{2.5}$ data from nearly 1500 ground stations in China into the model chemical initial fields to improve the model forecasts of the concentrations of PM2.5 and discuss the impact of assimilating $PM_{2.5}$ on visibility.

2 Methods and Data

2.1 The ensemble optimal interpolation algorithm

EnOI algorithm used in this study is based on the work of Evensen (2003). A brief recall of the EnKF and EnOI is given in this section. DA methods are algorithms that combine observations and model results and their respective statistical characteristics of errors to obtain a statistically optimal analysis value by minimizing the analysis variance. Based on Kalman filter theory, the analysis state $\boldsymbol{\psi}^a$ is determined by a linear combination of the vector of measurements $\boldsymbol{y}$ and the forecasted model state vector or background $\boldsymbol{\psi}^f$, which is given by the equation (1) and (2),

$$\boldsymbol{\psi}^a = \boldsymbol{\psi}^f + \boldsymbol{K}(\boldsymbol{y} - \boldsymbol{H}\boldsymbol{\psi}^f) \quad (1)$$

$$\boldsymbol{K} = \boldsymbol{P}\boldsymbol{H}^T[\boldsymbol{H}\boldsymbol{P}\boldsymbol{H}^T + \boldsymbol{R}]^{-1} \quad (2)$$

where $\boldsymbol{K}$ is Kalman gain matrix, $\boldsymbol{P}$ is the background error covariance matrix, $\boldsymbol{H}$ is the observation operator that relates the model state to the observation, and $\boldsymbol{R}$ is the observation error covariance matrix.

Now we define $\boldsymbol{A}$ is the matrix holding the ensemble members $\boldsymbol{\psi}_i$

$$\boldsymbol{A} = (\boldsymbol{\psi}_1, \boldsymbol{\psi}_2, \cdots, \boldsymbol{\psi}_N) \in \mathfrak{R}^{ndim \times N} \quad (3)$$

where $\boldsymbol{N}$ is the number of ensemble members and $\boldsymbol{ndim}$ is the size of the model state vector

let $\overline{\boldsymbol{A}}$ be the ensemble mean of $\boldsymbol{A}$, then the ensemble anomaly $\boldsymbol{A}'$ is defined as

$$\boldsymbol{A}' = \boldsymbol{A} - \overline{\boldsymbol{A}} \quad (4)$$

The ensemble covariance matrix P can be defined as

$$\boldsymbol{P} = \frac{\boldsymbol{A}'\boldsymbol{A}'^T}{\mathrm{N}-1} \in \mathfrak{R}^{ndim \times ndim} \quad (5)$$

the vector of measurements $\boldsymbol{y}$ need to be perturbed with its error as the following

$$\boldsymbol{d}_j = \boldsymbol{y} + \boldsymbol{\varepsilon}_j, \; j = 1, \cdots, N \quad (6)$$

which can be stored in a matrix as

$$\boldsymbol{D} = (\boldsymbol{d_1}, \boldsymbol{d_2}, \cdots, \boldsymbol{d_n}) \in \mathfrak{R}^{m \times N} \quad (7)$$

where m is the number of measurements.

The EnKF analysis equation will be expressed as the following

$$\boldsymbol{A}^a = \boldsymbol{A} + \boldsymbol{A}'\boldsymbol{A}'^T\boldsymbol{H}^T[(\boldsymbol{H}\boldsymbol{A}'\boldsymbol{A}'^T\boldsymbol{H}^T + (\mathrm{N}-1)\boldsymbol{R})]^{-1}(\boldsymbol{D} - \boldsymbol{H}\boldsymbol{A}) \quad (8)$$

The analysis includes updating each ensemble and need to run the model $\boldsymbol{N}$ times in every forecast cycle to calculate $\boldsymbol{P}$, therefore tends to be computationally demanding and has limited use when the computer time is the main affecter to be considered, especially in real-time operational forecast.

The EnOI analysis is computed with the ensemble covariance matrix $\boldsymbol{P}$ spanned by a stationary ensemble of model states sampled from a long-time integration. It is computed by solving an equation written as the following

$$\boldsymbol{\psi}^a = \boldsymbol{\psi}^f + \alpha\boldsymbol{A}'\boldsymbol{A}'^T\boldsymbol{H}^T[(\alpha\boldsymbol{H}\boldsymbol{A}'\boldsymbol{A}'^T\boldsymbol{H}^T + (\mathrm{N}-1)\boldsymbol{R})]^{-1}(\boldsymbol{y} - \boldsymbol{H}\boldsymbol{\psi}^f) \quad (9)$$

where the scalar $\alpha \in (0, 1]$ is introduced to allow for different weights on the ensemble versus measurements. As Evensen (2003) pointed out, an ensemble consisting of model states sampled over a long time period will have a climatological variance which is too large to represent the actual error in the model forecast, and α which mainly depends on how the model forecast behaviours is used to reduce the variance to a realistic level and can be tuned for optimal performance. In this study, it is taken as 0.9 based on our experience. Through Eq. (9) the EnOI analysis updates only one model state at a time, so the computer time can be reduced by one or two orders of magnitude.

2.2 The EnOI data assimilation system design

Using a set of ensemble forecasts with finite number to calculate the BEC will suffer from sample error and cause imperfect estimation or even filter divergence (Houtekamer and Mitchell, 1998). There are two sorts of techniques to possibly solve this problem. One is the distance-dependent covariance localization, which is done by updating the analysis at all grid points with the multiplication of the BEC by a correlation function (Hamill et al., 2001). The other is done by updating the analysis at each grid point simultaneously using the state variables and the observations in the local region centred at that point (Ott et al.2004). In our EnOI DA system, we use the second technique. First, we define the localization length-scale as L. For each model grid point, we find the observations within L which are called active observations, and then calculate the corresponding innovation. This localization effect on the analysis is illustrated in section 3.1 (Fig.3).

The observation error covariance matrix $\boldsymbol{R}$ is assumed to be diagonal here, that is, the observation errors are not correlated. The diagonal elements of $\boldsymbol{R}$ are thus given by the sum of the measurement error variance ε_o^2 and representativeness error variance ε_r^2 , following Elbern et al. (2007). The measurement error ε_o is assigned as 7.5% of observed value, and representativeness errors ε_r is formulated as $\varepsilon_r = \varepsilon_o \cdot \sqrt{\frac{\Delta x}{L_r}}$, where Δx is model grid resolution (10km in this study) and L_r is the characteristic representativeness length of the observation, defined as 2 km for urban sites, 10km for rural sites and 20km for remote sites, respectively.

Based on the Eq. (9), we built the EnOI initial field $PM_{2.5}$ assimilation system, as shown in Fig. 1. The main procedures can be divided into pre-processing, analysis, and post-processing. Pre-processing involves the acquisition of observed data and ensemble samples. Analysis is the revised main module of EnOI where the main computational processes are performed. Post-processing firstly verifies the assimilation results using the validation observations which are not used in EnOI and then processes the results obtained from assimilation into model-readable chemical initial conditions. Compared with the traditional EnOI, the time-continuous model historical forecast before the assimilation moment are selected as the ensemble samples for this study. The ensemble design is set to be as following: suppose the assimilation will be done at time t, first we evolve the model from the spin-up run at t-NΔt and integrate the model to time t (in our operational set up, Δt is 1 hour), therefore we get a time series of N hourly model forecast outputs A_{t-N+1}, A_{t-N+2}, …, A_{t-1}, A_t. These hourly outputs before the assimilation time t form the N-number ensemble $\boldsymbol{A}$, which can be used to calculate the average $\overline{\boldsymbol{A}}$ and anomalies $\boldsymbol{A'}$ and then the background error

covariance matrices $\boldsymbol{P}$ is calculated. The BEC is stationary for a particular analysis moment, but it changes with the assimilation moment during a long assimilation period. Because background error covariance statistics are derived directly from forecasts and the DA scheme does not need to modify the original CCMM, EnOI is very easy to apply and very cost-free in term of computation time.

2.3 GRAPES_Meso5.1/CUACE

In this study, the DA method EnOI was established for the latest updated version of the regional atmospheric chemistry model GRAPES_Meso5.1/CUACE developed by the China Meteorological Administration (Wang et al., 2022). The model system consists of two main components, which are called GRAPES_Meso and CUACE, respectively. GRAPES_Meso refers to a real-time operational weather forecasting model used by China Meteorological Administration (Chen et al., 2008; Zhang and Shen, 2008). Now, the new version of it has been established with the resolutions ranging from 3 to 10 km for regional forecast (Shen et al., 2020). It uses fully compressible non-hydrostatic equations as its model core. The vertical coordinates adopt the height-based, terrain-following coordinates, and the horizontal coordinates use the spherical coordinates of equal longitude–latitude grid points. The horizontal discretization adopts an Arakawa-C staggered grid arrangement and a central finite-difference scheme with second-order accuracy, while the vertical discretization adopts the vertically staggered variable arrangement. The time integration discretization uses a semi-implicit and semi-Lagrangian temporal advection scheme. The transport and advection processes for all gases and aerosols are calculated by the dynamic framework of it. The second component, CUACE, refers to the atmospheric chemistry model (the Chinese Unified Atmospheric Chemistry Environment model), which mainly includes three modules: the aerosol module (CAM), the gaseous chemistry module (RADM2) and the thermodynamic equilibrium module (ISOPIA). In the RADM2 module, 63 gas species through 21 photochemical reactions and 136 gas-phase reactions participate in the calculations. CAM module considers the dynamic, physical and chemical processes of aerosols including hygroscopic growth, dry and wet depositions, condensation, nucleation, vertical mixing, cloud chemistry, and coagulation and activation of cloud condensation nodules from aerosols.. Seven types of aerosols (sea salt, sand/dust, black carbon, organic carbon, sulfate, nitrate, and ammonium salt) are considered in the CAM. The aerosol size spectrum (except for ammonium salt) is divided into 12 bins with particles radium of 0.005–0.01, 0.01–0.02, 0.02–0.04, 0.04–0.08, 0.08–0.16, 0.16–0.32, 0.32–0.64, 0.64–1.28, 1.28–2.56, 2.56–5.12, 5.12–10.24, and 10.24–20.48 μm. The interface program that connects CUACE and GRAPES_Meso transmits the meteorological fields calculated in GRAPES_Meso and the emission data processed as needed to each module of CUACE. GRAPES_Meso and CUACE are online fully-coupled (Peng et al., 2021; Zhang et al., 2022).

2.4 Data

Based "Ambient air quality standards" (GB 3095-2012) of China, the mass concentration limit of $PM_{2.5}$ and its corresponding air quality level and air pollution index (API) are shown in Table 1. Haze is defined as a weather phenomenon caused by air pollution when visibility is less than 10km, according to "Observation and forecasting levels of haze" (QX/T 113-2010) of China. Three pollution episodes occurred in China in December 2016, with the most severe haze episode occurring in China from 16 to 21 December 2016 (see more details in Wang et al. 2022, Table 3). During this pollution episode, the highest daily $PM_{2.5}$ concentration peaks 600 μg m^{-3} in Shijiazhuang and some other cities, reaching the severely polluted level (250-500 μg m^{-3}). In this study, 15-23 December 2016 was selected as the main study period, and both model input data and observation data used in this study are within this month. Model input data include anthropogenic emission data, model meteorological initial and boundary data. The emission inventory used in this study is from the Multi-resolution Emissions Inventory for China (MEIC) in December 2016 (http://www.meicmodel.org/). The emission inventory covers power plants, industry (cement, Iron and steel, industrial boilers, petroleum industry), residential, transportation, solvent use and agriculture, in-field crop residue burning. National Centers for Environmental Prediction (NCEP) Final analysis (FNLs) data (https://rda.ucar.edu/datasets/ds083.3/) are used for the model's initial and 6 h meteorological lateral boundary input fields. The observations include $PM_{2.5}$ and visibility. Nearly 1500 ground-based hourly $PM_{2.5}$ (μg m^{-3}) observations from the Chinese Ministry of Environmental Protection, with the detailed location and spatial distribution of the stations shown in Fig. -2. The hourly meteorological automatic ground-based visibility data (km) were obtained from the China Meteorological Administration. The time format of these observations is processed to UTC and all the observational data are obtained after quality control and rechecked before use.

2.5 Experimental Setup

The horizontal resolution, time step, forecast length and model domain of the GRAPES_Meso5.1/CUACE model are optional. In this study, the horizontal resolution of the model is 0.1°×0.1°, the time step is 100 s considering model integration stability and accuracy, and the model domain is15-60° E, 70-145° N and (grey dashed box in Figure 2). There are 49 model layers ascending vertically from the surface to 31km in height. The model warm restart time is 0000 UTC and 1200 UTC, and the forecast length is 24 hours. The model simulation results are output on an hourly basis.

Three groups of experiments were performed in this study: one set of control experiments (CR), one set of sensitivity experiments and one set of cyclic DA experiments, as shown in Table 1. CR00 is the control experiment representing model run without DA begin at 0000 UTC every day and forecast 24 hours (the initial field is the previous day's 24-hour forecast field), simulated from 1 to 31 December 2016. CR12 is also model run without DA but begins at 1200 UTC every day and forecast 24 hours. The localisation length-scale L and the ensemble size N are the key parameters affecting EnOI. Based on CR00, two parallel sensitivity experiments were designed to study the impact of localisation length-scale and ensemble size on the assimilation effects. The chemical initial fields, ensemble samples for the sensitivity experiments were obtained from

the CR00. The first group of sensitivity experiments is fixed with ensemble size N of 48, and length-scale is selected for 20, 40, 60, 80, and 100 km to investigate the impacts of different localization length-scale choices on the optimized chemical initial field; the second group is fixed with length-scale L of 80 km, and the 24, 48, 72, 96, 120, and 144 simulations before the assimilation moment (0000 UTC) were selected as ensemble samples, respectively, and the effect of the number of ensemble samples on the assimilation effect was discussed.

To investigate the impact of the assimilation moment on the forecast fields, the optimal length-scale and ensemble size were selected based on the results of sensitivity experiments, and two sets of cyclic DA experiments, DA00 and DA12, were set up to represent the daily assimilation of the initial fields at 0000 UTC and 1200 UTC, respectively. The N hourly model forecasts before the assimilation moment were used as the ensemble samples to approximate the BEC, and the analysis increments are calculated by combining the model forecasts and $PM_{2.5}$ observations at 0000 UTC and 1200 UTC, and the analysis are used as the chemical initial fields for the next forecast to achieve cyclic DA.

3 Result and discussion

3.1 Localization length-scale sensitivity experiments

The localization effect on the analysis is illustrated firstly and two observation sites A (114.5° E, 38.0° N), and B (36.6° N, 116.9° E) were selected to perform a length-scale single-point experiment for the initial field at 0000 UTC on 15 December 2016, corresponding to the left and right columns of the analysis increments ($\boldsymbol{\psi}^a - \boldsymbol{\psi}^f$) shown in Fig. 3. The analysis increments are determined by both the observation increments and the BEC based on Eq. (9). As shown in Fig. 3, the increments are positive in the left and negative in the right column, which represent the underestimation of $PM_{2.5}$ concentration at site A and overestimation at site B before being assimilated. As the length-scale increases, the range of analysis increment expands, and the number of model grids that can be affected increases gradually. Due to the sparse distribution of $PM_{2.5}$ sites, if the localization length-scale is too small, most of the model grids cannot be updated, which reduces the assimilation efficiency; whereas if the localisation length-scale is too large, the analysis increments between distant sites will offset and superimpose, creating fake increments. With the experiments using length-scale of L = 80 and 100 km, a small negative analysis increments are found at site A in the southeast direction. Compared to site A, a wide positive analysis increments that do not match the actual situation are found at site B in the west direction for experiments using L=60, 80, and 100km. It is worth noting that there are differences in the shape of the analysis increment fields at sites A and B, which is related to the EnOI having a flow-dependent BEC, the details of BEC will be discussed in 3.2.

Ground-based $PM_{2.5}$ sites are established according to the population and economic development level of the region, and are not evenly distributed, such as Beijing, Shanghai, Guangzhou, and other economically developed and populous megacities, which have a high density of $PM_{2.5}$ sites, while the western and central regions of China are sparsely populated, and the sites are partially sparse. So, in order to obtain the statistically optimal localization length-scale, we performed assimilation experiments on the initial fields at 0000 UTC each day from 1 to 31 December. 50% of $PM_{2.5}$ sites were randomly selected as

DA sites, and the rest were used as verification sites (without DA), and the blue and brown sites shown in Fig. 2 represent the spatial distribution of verification and assimilation sites, respectively. The statistics results of verification sites against the observation are shown in Table 3. Compared to the CR, Correlation Coefficient (CORR) of DA for verification sites increase from 0.65 to 0.77 at least, and the Root Mean Square Error (RMSE), Mean Bias (MB), and Mean Error (ME) of the DA experiment are smaller than those of the CR. The statistical data are different for different Localisation length-scale, indicating that localization can have an effect on the assimilation. Compared with the CR, RMSE of DA decreased from 60.1 to 41.6 μg m^{-3},MB decreased from 8.5 to 3.2 μg m^{-3} and ME decreased from 41.73 to 25.9 μg m^{-3} for the localization length-scale selection of 40 km, which is the best among all the experiments on different length-scale. Localisation length-scale of 60km and 80km have similar statistics results, but the statistics of 20km and 100km are not very good. Using a localization length-scale of 20 km prevents most of the model data from being updated while using too large a length-scale allows remote sites to interact with each other and produce more spurious increments. In addition, from the meteorological conditions, heavy pollution weather is always characterized by small or static winds, pollutant transport over small distances, an observation site represents a limited spatial extent, so a larger localized length-scale setting may also not produce a very realistic initial field. From this sensitivity experiment, we find that when the localization length-scale is using from 40 km to 80km, the statistics are relatively good and the optimal assimilation effect can be achieved.

3.2 Ensemble size sensitivity experiments

We repeat the series of experiments presented in Fig. 3, but with a localising length-scale of 80 km and 24, 48, 72, 96 and 120 ensemble members. Figure 4 shows a map of BEC correlation field between observation sites (A, B) for different ensemble size, overlaid with the 0000 UTC surface wind vector of 15 December 2016. Site A is controlled by strong north and northwest winds, which makes the CORR field show a northeast-southwest trend; The wind speed at site B is less than 5 $m.s^{-1}$ in all directions with a steady state, so the CORR field is approximately distributed in concentric circles nearby the center of the site. As the number of ensemble samples increases, the area of positive CORR greater than 0.7 gradually increases in A and B.. The ensembles of size N =24 or N=48 can be considered small compared to the selection of other ensemble sizes in sensitivity experiments. In this case, the CORRs between the observation sites and the surrounding large-scale areas are all greater than 0.7, and an extremely strong negative correlation is found in the southwest. The success of ensemble-based DA systems depends strongly on the number of samples. The smaller ensemble size fails to accurately estimate the BEC and is prone to sampling error, resulting in an overestimation or underestimation of the initial field, and Natvik and Evensen (2003) investigated the effect of the number of samples on assimilation and showed that an ensemble of fewer than 60 samples reduce the performance of assimilation. When the hourly model forecasts of over 5 days (N=120) before assimilation are selected as the ensemble samples, the correlations of both sites A and B with the BECs in a wide area become positive.

The DA sites were used to assimilate the initial field at 0000 UTC per day for December 2016, and six different ensemble sizes were used to improve the initial field as shown in table 4. Compared with the initial field without data assimilation, the RMSE, CORR, MB, and ME of the initial field after assimilation had all been improved and the improvement were different

depending on the ensemble size. The priori initial field is shown in table 4 "CR". With only 24 ensemble samples assimilated, the RMSE of verification sites decreased from 60.1 to 48.6 μg m^{-3}, the CORR increased from 0.56 to 0.76, and the MB and ME are decreased from 8.5 to 4.2 μg m^{-3} and 41.7 to 30.8 μg m^{-3}, respectively. As seen in table 3 the statistics of verification sites become progressively better as the ensemble members increases from 24 to 48, 72, and 96. The verification sites RMSEs for 48, 72, and 96 samples are 44.9, 42.4 and 40.70 μg m^{-3} respectively, the CORRs are 0.80, 0.81, 0.82, and the MEs are 27.0, 25.9, and 25.7. When 120 samples or 144 samples were selected for assimilation, the analysis field $PM_{2.5}$ DA and verification statistics were not better than those of 96 samples. The verification sites RMSEs for 120, and 144 samples were 44.1, and 45.8 μg m^{-3} respectively, and the CORRs also became smaller. The differences between the statistics also indicate there is an optimal ensemble size, the RMSE of the experiment using 96 samples is smaller than the RMSE when using the other ensemble sizes, and the remaining statistics are better than the results when other samples are selected, so we consider that in this sensitivity experiments the best assimilation is achieved when the number of ensemble size is 96. It is noted from the experimental results that not the larger the ensemble, the better the results in this study. It could be influenced by the following reasons that the atmospheric chemistry model used in the study is coupled online with the mesoscale regional weather model GRAPES_Mese5.1. The mesoscale regional weather model differs from the climate model and the global model in that the mesoscale model represents weather systems on time scales of one day to several days(Emanuel, 1986). In addition, atmospheric chemical processes are fast-varying processes with small time scales compared to climatic and oceanic processes, so using model results from long-time integrations as ensemble may average out the "error of the day" and will not be a very good assessment of model background errors.

3.3 Impact on initial fields

In order to verify the assimilation effect and evaluate quantitatively the impact of the EnOI system on the initial fields, DA experiments with length-scale of L=40 and ensemble size of N= 96 was performed on the initial field at each 0000 UTC from 15 to 23 December 2016. The assimilated observations were obtained from the DA sites in Fig. 2, and the effect on both DA sites and verification sites are evaluated. Figure 5 shows the statistics for the two regions of the initial field, the China mainland, and North China. In China mainland, the CORRs of the verification sites and DA sites before assimilation were 0.60 and 0.58, respectively, and the RMSEs were 73.9 and 73.4 μg m^{-3}, respectively. After the DA sites were assimilated, the CORR of assimilated sites increased to 0.99 and the RMSE decreased to 14.5 μg m^{-3}, and the CORR of verification sites increased to 0.84 and the RMSE decreased to 46.4 μg m^{-3}, meanwhile the ME changes from 49.7 to 27.3 μg m^{-3}. In North China, after the DA sites were assimilated, each statistic of the validation site also changed, with the CORR increasing from 0.53 to 0.87, RMSE decreasing from 105.5 to 65.7 μg m^{-3}. Only 50% of the ground-based observation are assimilated and the statistics of the validation sites also have been improved. This experimental results prove that the DA system can indeed yield more accurate initial field with over 40% increase of CORR and 37% reduction of RMSE

To illustrate the assimilation effect of different pollution levels, we consider this episode from 15 to 23 December 2016, in which the first two days as the pollution start period, days 3 to 7 as the pollution period, and the last two days as the pollution dissipation period. We compared the $PM_{2.5}$ observations and initial conditions before and after DA within all the observations sites assimilated during this episode. This was done to understand the impact of DA for initial conditions in the system's actual operating situation. Fig. 6 shows the spatial distribution of $PM_{2.5}$ in the observation field (OB), background field (BF), analysis field (AF), and analysis field increments (AFI) for two days of light pollution (16 and 23 Dec.) and two days of heavy pollution (19 and 20 Dec.). The black boxed area in Fig.6 is the same as North China (NC) in Fig. 2, including Beijing, Tianjin, eastern Shanxi, southern Hebei, western Shandong, and northern Henan, which has the highest simulated $PM_{2.5}$ concentration. Table 5 summarizes the corresponding statistics of initial $PM_{2.5}$ concentrations for assimilation sites and verifications sites before and after EnOI. Fig. 6 shows that, compared with OBs, the model background $PM_{2.5}$ without DA can capture the spatial pattern of distribution over China in general which shows that the model performance is moderate good. However, there are still errors between the background and observations. $PM_{2.5}$ concentrations are overestimated in NC and eastern China during the pollution start and dissipation periods. During the heavy pollution period, the background $PM_{2.5}$ concentrations are overestimated in northeast China and underestimated in NC. After assimilating the ground-based $PM_{2.5}$, the $PM_{2.5}$ concentration increments were distributed around the observation sites as expected and were more closer to the observations distributions. Negative values of the AFI demonstrate that assimilation reduces $PM_{2.5}$ concentrations, while positive values demonstrate that assimilation increases $PM_{2.5}$ concentrations. During the period before and after pollution, $PM_{2.5}$ concentrations decrease in eastern China and increase in western China and NC, indicating a reduction in over- or under-prediction of model $PM_{2.5}$ concentrations after assimilation. Table 5 shows that assimilating 50% of the ground-based observations improved the initial condition for other areas where have no assimilated sites. Take 19 Dec. 2016 as an example, the CORR for verification sites increased from 0.66 to 0.85, RMSE decreased from 79.2 to 56.1μg m^{-3}, and MB and ME also became smaller after EnOI. These results indicate that the initial PM_{25} fields can be adjusted efficiently by EnOI. What is the impact of this innovation through the EnOI system for $PM_{2.5}$ forecast is discussion in the next section.

3.4 Impact on forecast fields

3.4.1 Impact on $PM_{2.5}$ forecast fields

In this section, we will discuss the impact of assimilation observations on $PM_{2.5}$ forecasts. As in Section 3.3, we assimilate the DA sites at 0000 UTC from 15 to 23 December 2016, and then analyse the following forecast of DA and the verification sites separately. The RMSE of the DA and verification sites in China mainland and North China for a complete pollution process obtained average over 15 to 23 December 2016 is shown in Fig. 7. For the DA sites in China mainland (Fig.7a), the model forecast RMSE without DA is about 75 μg m^{-3}, after the assimilation, the model forecasts RMSE is decreased rapidly from 75.4 to 40.1μg m^{-3}, which is an over 40% reduction. This implies that assimilation with EnOI can considerably improve the forecast accuracy. Meanwhile, it is notable that assimilation of DA sites also has an impact on the forecast at the verification

sites. The trend of the RMSE series at the verification site is consistent with the DA site, but smaller in values. The RMSE of verification sites at 1h forecast hour dropped from 75.5 to 51.0 μg m^{-3}, about 32% reduction. For North China, which was shown in Figure7c and d, the model forecast RMSE without DA is about 115 μg m^{-3}. After the assimilation of $PM_{2.5}$ observation, the model forecasts RMSE of DA sites at 1h forecast time is decreased rapidly from 122 to 56.1μg m^{-3}, which is an over 54% reduction. For verification sites, the reduction amplitude is 33%, smaller than that of DA sites, but still a moderate improvement considering only 50% ground-based observations were used to be assimilated at 0000UTC. The results show that assimilation with EnOI not only improve the forecast for the DA sites but also the verification sites. The improvements are mainly within the first 12h forecasts with an RMSE greater than 10 μg m^{-3}. The improvement receded with forecast time, changing from 46% at 1h forecast hour to 7% at 24h forecast hour. These results are consistent with previous study, which either used 4DVAR or EnKF (Wu et al. 2008; Bocquet et al, 2015, Park et al.,2022). As Bocquet et al. (2015) pointed out, even with the improved analysis, the impact of initial state adjustment is generally limited to the first day of the forecast, for pollutant transport and transformation are strongly driven by uncertain external parameters, such as emissions, deposition, boundary conditions, and meteorological fields.

Now we use all ground-based observation sites as DA sites to investigate the performance of assimilating the initial field at 0000 UTC per day (DA00) or 1200 UTC per day (DA12) on improving the $PM_{2.5}$ forecasts. DA00 and DA12 were performed in parallel. The daily average of the 24-hour RMSE was obtained for the DA and CR experiments. Rate of improvement (ROI) by data assimilation in 1d (24h) predictions for 15 to 23 December 2016 for Mainland China and NC were calculated using the ratio of the reduced RMSE statistical metrics to those for the CR simulation and plotted in a daily time series histogram as shown in Fig. 8. In this episode, the improvement of China mainland $PM_{2.5}$ forecasts by DA00 and DA12 are minimum at 9% and 10% respectively on December 15 and maximum at 15% and 21% respectively on December 19. The minimum and maximum improvement of assimilation on $PM_{2.5}$ forecasts in NC both appear in DA12, which are 4% and 25%, respectively. The difference between DA12 and DA00 relative RMSEs is mostly positive, within 6% in China mainland, but in NC this difference can be up to 15%. The average RMSE improvement of 24h forecast for China mainland and the North China assimilation at 0000 UTC is 12.3% and 9.8%, respectively, while that at 1200 UTC is 14.4% and 14.0%, respectively. In terms of the average relative RMSE for this episode, assimilating the initial field at 1200 UTC improves the $PM_{2.5}$ forecast more than 0000 UTC, mainly because the model forecasts are not close to the observations at 1200 UTC in most cases, thus choosing this time for assimilation will have a significant impact. In addition, the DA effect varies for each day and the larger the error, the greater the improvement in RMSE from DA, which means that the larger the a priori error, the greater the improvement from DA. These results show that using EnOI to assimilate ground-based $PM_{2.5}$ observations for the model chemical initial field can reduce over 9.8% of RMSE for 24h forecast in average. Park et al. (2022) implemented an ensemble Kalman filter in the Community Multiscale Air Quality model (CMAQ model v5.1) for data assimilation of ground-level $PM_{2.5}$. They found using EnKF with 40 ensemble number can reduce 9.6% of RMSE for 24h forecast. Comparing their results with ours, we can find that, while EnOI is sub-optimal, it can give improvement of forecast that are comparable to those of the EnKF. Moreover, the computational cost of EnOI is typically about N times less than that of EnKF. Therefore, we suggest that EnOI may provide

a practical and cost-effective alternative to the EnKF for the applications where computational cost is a main limiting factor, especially for real-time operational forecast.

To achieve better performance of assimilation, we update the initial field every 12h. Figure 9 gives time series of forecasts and observations in term of $PM_{2.5}$, together with RMSE of CR and DA for North China. Compared with the observations, the forecast $PM_{2.5}$ concentrations are 20 to 100 μg m^{-3} higher in the pollution start period (15-17 December) and the pollution fading period (21, 23 December), about 100 μg m^{-3} lower on December 19. The $PM_{2.5}$ concentrations changes immediately one hour after 0000 UTC or 1200 UTC. It can be seen from Fig. 9b, the RMSEs of the DA experiments are always lower than that of the CR experiments, and the difference in RMSE between the CR and DA experiments receded with forecast time. This proves that assimilating the initial field can improve the $PM_{2.5}$ forecast. Note that the DA algorithm used here cannot produce an optimal solution when there are larger errors in the model. On 19 December 2016, even with DA the model still cannot retrieve the true variation very well for the first 12 hour forecast. This suggest that using DA on initial field can only partially remedy inherent model error. To improve the analysis capabilities and prolong the impact of DA on $PM_{2.5}$ forecasts, we should extend the assimilation for adjusting emissions, meteorological field and other model uncertainty sources.

3.4.2 Impact on Visibility forecast fields

The occurrence of low visibility episodes is usually associated with aerosol pollution. The horizontal spatial distribution of the OBs, forecast fields without assimilation (CR), forecast fields with assimilation (DA), and incremental fields (DA-CR) for visibility and $PM_{2.5}$ at 0100 UTC on 16 and 20 December are shown in Fig.10. During the pollution start period (16 December 0100 UTC) visibility is above 10km in most of China, and during the pollution period (20 December 0100 UTC) visibility is mostly below 7km in eastern China. After assimilating the ground-based $PM_{2.5}$, the visibility distribution of DAs more consistent with the observation compared to the CRs. A positive $PM_{2.5}$ concentration increment corresponds to a negative visibility increment, that means that when the $PM_{2.5}$ concentration increases, the visibility decreases at the same moment. At 0100UTC On 16 December, the CR $PM_{2.5}$ concentration is underestimated in NC and overestimated in Southeast China, and after assimilating $PM_{2.5}$, the visibility is reduced in NC with increased $PM_{2.5}$ and increased in Southeast with reduced $PM_{2.5}$. In the period of light pollution, the absolute value of visibility increment is mostly in the range of 5-7 km when the $PM_{2.5}$ increment is from 30 to 110 μg m^{-3} or from -30 to -110 μg m^{-3} in NC, while in the pollution period (20 December 0100 UTC for example), under the same $PM_{2.5}$ analysis increment, the visibility increment in NC is between -3 and 3 km.

Four stations, Beijing (BJ), Shijiazhuang (SJZ), Xingtai (XT), and Jinan (JN), were selected from the heavily polluted NC to study the effect of assimilating the initial field $PM_{2.5}$ on the visibility forecasts. Since the assimilation effect is most obvious in the first 12 hours, we focus on the improvement of visibility forecasts within 12 hours. Figure 11 shows the observation, simulation and assimilation of visibility and observation, simulation and assimilation of $PM_{2.5}$ concentration for the above cities from 0100 to 1200 on 16 and 20 December 2016. On 16 December, when $PM_{2.5}$ concentration is less than 300 μg m^{-3} (December 16), visibility at all four stations is closer to the observed value by assimilating $PM_{2.5}$, among which BJ and JN

have decreased $PM_{2.5}$ concentration after assimilation, and visibility has increased at the same time. SJZ and XT have increased $PM_{2.5}$ concentration and decreased visibility after assimilation. In the period of low $PM_{2.5}$ concentration, about 100 μg m^{-3} $PM_{2.5}$ change makes visibility change 11km, 4km, 5km and 7km in BJ, SJZ, XT and JN respectively. In the period of heavy pollution, $PM_{2.5}$ concentration change 150 μg m^{-3} in Beijing and Shijiazhuang at 0100UTC, while visibility change 3.5km and 0.5km respectively. These result show that the improvement of visibility by assimilating $PM_{2.5}$ is limited during the heavy pollution period. It is worth noting that when the $PM_{2.5}$ concentration is greater than 350 μg m^{-3} at the JN site, although the decrease of $PM_{2.5}$ concentration corresponds to the increase in visibility, the gap between the assimilated visibility and observation becomes larger at this time, which may be related to the inaccuracy of the humidity simulation here and inaccurate visibility parameterization scheme for the model. Visibility is not linearly related to $PM_{2.5}$, and visibility is also affected by humidity and other factors. Assimilation of the initial field $PM_{2.5}$ can improve the visibility forecast, but if we want to improve the visibility forecast significantly, we need to improve not only the visibility parameterization scheme, but also the humidity accuracy.

4 Conclusions

To improve the accuracy of $PM_{2.5}$ and visibility forecasting in China, a real-time and efficient EnOI assimilation system is established for the latest online operational chemistry weather model GRAPES_Meso5.1/CUACE of China Meteorological Administration. The ground-based $PM_{2.5}$ observation data nearly 1500 surface stations covering the whole country are used for assimilation. $PM_{2.5}$ and visibility simulation-assimilation experiments were performed for a haze pollution episode from 15 to 23 December 2016. Parallel sensitivity experiments of localization length-scale and ensemble size were set up to determine two key parameters that influence the effectiveness of EnOI assimilation. Based on the results of sensitivity experiments, the initial fields were assimilated at 0000 UTC each day from 15 to 23 December 2016 to study the improvement of EnOI on the initial field $PM_{2.5}$. In addition to the analysis of the China mainland assimilation effect, the heavily polluted North China was additionally divided to discuss the different impacts of assimilation on the overall and regional chemical initial fields. Cyclic assimilation experiments were performed at 0000 UTC (DA00) and 1200UTC(DA12) to investigate the impacts of assimilation on the forecast fields, taking NC as an example, to discuss the impacts of assimilation on $PM_{2.5}$ and visibility forecast fields.

The optimal localization length-scale and the number of ensemble samples are 40 km and 96, respectively, derived from sensitivity experiments. Assimilating 50% of the ground-based observations improved the initial condition for other areas where have no assimilated sites. The DA can considerably improve the model $PM_{2.5}$ initial field, the CORR of verification sites in mainland China improved from 0.58 to 0.84 and the RMSE decreased from 73.7 to 46.4 μg m^{-3}, respectively. The results of the DA00, DA12 assimilation experiments showed that the improved impacts of the DA worked throughout the forecast time window, but the assimilation impact was most pronounced in the first 12 hours and gradually decreased in the subsequent time. Within the 24-hour forecast time window, the average RMSE improvement for the China mainland $PM_{2.5}$

forecast field ranges from 9% to 21%, and between 4% and 25% in NC, and the comprehensive comparison shows that the initial field of 1200 UTC assimilation is superior to 0000 UTC. Therefore, in this study, it is considered that with limited computational resources, the EnOI assimilation efficiency is highest with the largest distance between the model simulation and observation to assimilate according to the model characteristics. When it comes to operational use, the assimilation efficiency can be improved by shortening the assimilation time interval due to the small demand of EnOI computational resources.

The assimilation of $PM_{2.5}$ also has a positive impact on visibility forecasts. When the $PM_{2.5}$ increment by assimilation is negative, it corresponds to an increase in visibility, and when the $PM_{2.5}$ analysis increment is positive, visibility decreases correspondingly. The greater the change in $PM_{2.5}$ concentration during periods of light pollution, the more pronounced the improvement in visibility. It is worth noting that visibility is also related to a variety of factors and assimilating only ground-based $PM_{2.5}$ sites has a limited effect on visibility, and we will further consider assimilating PM_{10}, humidity and other meteorology factors to improve visibility forecasts in subsequent studies.

Code and data availability. The EnOI method and related processes written in Fortran language and observation data used in this research are available at https://doi.org/10.5281/zenodo.7002847. The National Centers for Environmental Prediction Global Final Analysis (NCEP-FNL) data are available online (https://rda.ucar.edu/datasets/ds083.2/ and https://rda.ucar.edu/datasets/ds083.3/). The emission inventories are available online (http://www.meicmodel.org/).

Author contributions. LST: Validation, Formal analysis, Writing - Original Draft, Visualization, Investigation, Software. WP: Conceptualization, Methodology, Software, Writing - Original Draft. WH: Conceptualization, Methodology, Supervision, Writing- Reviewing and Editing. PY: Validation, Software. LZD and ZWJ: Validation. LHL: Data Curation. WYQ and CHZ: Resources. ZXY: Supervision

Competing interests. The contact author has declared that neither they nor their co-authors have any competing interests.

Acknowledgements. This study is supported by the National Key Research and Development Program（2019YFC0214603, 2019YFC0214601) and the NSFC for distinguished young scholars (41825011). We also appreciate the comments of the reviewers that helped us to improve this article.

References

Benedetti, A., Reid, J. S., Knippertz, P., Marsham, J. H., Di Giuseppe, F., Rémy, S., Basart, S., Boucher, O., Brooks, I. M., Menut, L., Mona, L., Laj, P., Pappalardo, G., Wiedensohler, A., Baklanov, A., Brooks, M., Colarco, P. R., Cuevas, E., da Silva, A., Escribano, J., Flemming, J., Huneeus, N., Jorba, O., Kazadzis, S., Kinne, S., Popp, T., Quinn, P. K., Sekiyama, T. T., Tanaka, T., and Terradellas, E.: Status and future of numerical atmospheric aerosol prediction with a focus on data requirements, Atmos. Chem. Phys., 18, 10615–10643, 10.5194/acp-18-10615-2018, 2018

Bocquet, M., Elbern, H., Eskes, H., Hirtl, M., Žabkar, R., Carmichael, G. R., … Seigneur, C.: Data assimilation in atmospheric chemistry models: current status and future prospects for coupled chemistry meteorology models. Atmospheric Chemistry and Physics, 15(10), 5325–5358, 10.5194/acp-15-5325-2015,2015.

Carnevale, C., De Angelis, E., Finzi, G., Turrini, E., and Volta, M.: Optimal Interpolation Based Data Fusion Techniques to Improve Deterministic Air Quality Forecast, Air Pollution Modeling and its Application XXVII, Berlin, Heidelberg, 145-150, 10.1007/978-3-662-63760-9_22, 2021

Castruccio, F. S., Karspeck, A. R., Danabasoglu, G., Hendricks, J., Hoar, T., Collins, N., and Anderson, J. L.: An EnOI-Based Data Assimilation System With DART for a High-Resolution Version of the CESM2 Ocean Component, Journal of Advances in Modeling Earth Systems, 12, 10.1029/2020ms002176, 2020.

Chen, D., Liu, Z., Fast, J., and Ban, J.: Simulations of sulfate–nitrate–ammonium (SNA) aerosols during the extreme haze events over northern China in October 2014, Atmospheric Chemistry and Physics, 16, 10707-10724, 10.5194/acp-16-10707-2016, 2016.

Cheng, Y., Dai, T., Goto, D., Schutgens, N. A. J., Shi, G., and Nakajima, T.: Investigating the assimilation of CALIPSO global aerosol vertical observations using a four-dimensional ensemble Kalman filter, Atmospheric Chemistry and Physics, 19, 13445-13467, 10.5194/acp-19-13445-2019, 2019.

Counillon, F. and Bertino, L.: Ensemble Optimal Interpolation: multivariate properties in the Gulf of Mexico, Tellus A: Dynamic Meteorology and Oceanography, 61, 296-308, 10.1111/j.1600-0870.2008.00383.x, 2009.

Dai, T., Cheng, Y., Suzuki, K., Goto, D., Kikuchi, M., Schutgens, N. A. J., Yoshida, M., Zhang, P., Husi, L., Shi, G., and Nakajima, T.: Hourly Aerosol Assimilation of Himawari-8 AOT Using the Four-Dimensional Local Ensemble Transform Kalman Filter, Journal of Advances in Modeling Earth Systems, 11, 680-711, 10.1029/2018ms001475, 2019.

Elbern H, Strunk A, Schmidt H, Talagrand O..: Emission rate and chemical state estimation by 4-dimensional variational inversion [J]. Atmospheric Chemistry and Physics, 7 (1): 3749–3769, 10.5194/acp-7-3749-2007, 2007.

Evensen, G.: The Ensemble Kalman Filter: theoretical formulation and practical implementation, Ocean Dynamics, 53, 343-367, 10.1007/s10236-003-0036-9, 2003.

Feng, S., Jiang, F., Jiang, Z., Wang, H., Cai, Z., and Zhang, L.: Impact of 3DVAR assimilation of surface PM2.5 observations on PM2.5 forecasts over China during wintertime, Atmospheric Environment, 187, 34-49, 10.1016/j.atmosenv.2018.05.049, 2018.

Fu, W. and Zhu, J.: Effects of Sea Level Data Assimilation by Ensemble Optimal Interpolation and 3D Variational Data Assimilation on the Simulation of Variability in a Tropical Pacific Model, Journal of Atmospheric and Oceanic Technology, 28, 1624-1640, 10.1175/jtech-d-11-00044.1, 2011.

Ghorani-Azam, A., Riahi-Zanjani, B., and Balali-Mood, M.: Effects of air pollution on human health and practical measures for prevention in Iran, J Res Med Sci, 21, 65, 10.4103/1735-1995.189646, 2016.

Gong, S. L. and Zhang, X. Y.: CUACE/Dust – an integrated system of observation and modeling systems for operational dust forecasting in Asia, Atmos. Chem. Phys., 8, 2333-2340, 10.5194/acp-8-2333-2008, 2008.

Ha, S.: Implementation of aerosol data assimilation in WRFDA (v4.0.3) for WRF-Chem (v3.9.1) using the RACM/MADE-VBS scheme, Geosci. Model Dev., 15, 1769–1788, 10.5194/gmd-15-1769-2022, 2022.

Hamill T.M., Whitaker J.S., Snyder C.: Distance-dependent filtering of background error covariance estimates in an ensemble Kalman filter. Mon. Weather Rev. 129, 2776–2790, 10.1175/1520-0493(2001)129<2776:DDFOBE>2.0.CO;2, 2001.

Houtekamer, P. L., and Mitchell H. L., 1998: Data assimilation using an ensemble Kalman filter technique. Mon. Wea. Rev., 126, 796–811, 10.1175/1520-0493(1998)126<0796:DAUAEK>2.0.CO;2, 1998.

Hu, X., Waller, L. A., Al-Hamdan, M. Z., Crosson, W. L., Estes, M. G., Jr., Estes, S. M., Quattrochi, D. A., Sarnat, J. A., and Liu, Y.: Estimating ground-level PM(2.5) concentrations in the southeastern U.S. using geographically weighted regression, Environ Res, 121, 1-10, 10.1016/j.envres.2012.11.003, 2013.

Kalnay E: Atmospheric modeling, data assimilation and predictability[M]. Cambridge university press, 10.1017/CBO9780511802270, 2003.

Kong L., et al.: A Fast Emission Inversion Scheme Based on Ensemble Optimal Interpolation [J]. Climatic and Environmental Research (in Chinese), 26 (2): 191−201. 10.3878/j.issn.1006-9585.2020.20043, 2021.

Lee, L. A., Reddington, C. L., and Carslaw, K. S.: On the relationship between aerosol model uncertainty and radiative forcing uncertainty, Proc Natl Acad Sci U S A, 113, 5820-5827, 10.1073/pnas.1507050113, 2016.

Li, Z., Zang, Z., Li, Q. B., Chao, Y., Chen, D., Ye, Z., Liu, Y., and Liou, K. N.: A three-dimensional variational data assimilation system for multiple aerosol species with WRF/Chem and an application to PM_{2.5} prediction, Atmospheric Chemistry and Physics, 13, 4265-4278, 10.5194/acp-13-4265-2013, 2013.

Lin, C., Wang, Z., and J, Z.: A data assimilation method of the Ensemble Kalman Filter for use in severe dust storm forecasts over China, Atmospheric Chemistry and Physics Discussions, 7, 10.5194/acpd-7-17511-2007, 2007.

Liu, C., Zhang, S., Gao, Y., Wang, Y., Sheng, L., Gao, H., and Fung, J. C. H.: Optimal estimation of initial concentrations and emission sources with 4D-Var for air pollution prediction in a 2D transport model, Sci Total Environ, 773, 145580, 10.1016/j.scitotenv.2021.145580, 2021.

Liu, F., Tan, Q., Jiang, X., Yang, F., and Jiang, W.: Effects of relative humidity and $PM_{2.5}$ chemical compositions on visibility impairment in Chengdu, China, Journal of Environmental Sciences, 86, 15-23, 10.1016/j.jes.2019.05.004, 2019.

Liu H.，Rao X. Q.，Zhang H. D.，Li M. and Zhang Z. G.: Comparative verification and analysis of environmental meteorology operational numerical prediction models in China, Journal of Meteorology and Environment, 33 (5),17-24, 2017.
Liu, Z., Liu, Q., Lin, H.-C., Schwartz, C. S., Lee, Y.-H., and Wang, T.: Three-dimensional variational assimilation of MODIS aerosol optical depth: Implementation and application to a dust storm over East Asia, Journal of Geophysical Research: Atmospheres, 116, 10.1029/2011JD016159, 2011.
Natvik, L. J. and Evensen, G.: Assimilation of ocean colour data into a biochemical model of the North Atlantic: Part 1. Data assimilation experiments, Journal of Marine Systems, 40-41, 127-153, 10.1016/S0924-7963(03)00016-2, 2003.
Navon, I. M.: Data Assimilation for Numerical Weather Prediction: A Review, in: Data Assimilation for Atmospheric, Oceanic and Hydrologic Applications, edited by: Park, S. K., and Xu, L., Springer Berlin Heidelberg, Berlin, Heidelberg, 21-65, 10.1007/978-3-540-71056-1_2, 2009.
Oke, P., Brassington, G., Griffin, D., and Schiller, A.: Ocean Data Assimilation: a case for ensemble optimal interpolation, Australian Meteorological and Oceanographic Journal, 59, 10.22499/2.5901.008, 2010.
Oke, P. R., Sakov, P., and Corney, S. P.: Impacts of localisation in the EnKF and EnOI: experiments with a small model, Ocean Dynamics, 57, 32-45, 10.1007/s10236-006-0088-8, 2007.
Oke, P. R., Allen, J. S., Miller, R. N., Egbert, G. D., and Kosro, P. M.: Assimilation of surface velocity data into a primitive equation coastal ocean model, Journal of Geophysical Research: Oceans, 107, 5-1-5-25, 10.1029/2000JC000511, 2002.
Pagowski, M. and Grell, G. A.: Experiments with the assimilation of fine aerosols using an ensemble Kalman filter, Journal of Geophysical Research: Atmospheres, 117, 10.1029/2012JD018333, 2012.
Ott E., Hunt B.R., Szunyogh I., Zimin A.V., Kostelich E.J., Corazza M.,Kalnay E., Patil D. J., Yorke J.A.: A local ensemble Kalman filter for atmospheric data assimilation. Tellus 56A:415–428, 10.1111/j.1600-0870.2004.00076.x, 2004.
Park, S. Y., Dash, U. K., Yu, J., Yumimoto, K., Uno, I., and Song, C. H.: Implementation of an ensemble Kalman filter in the Community Multiscale Air Quality model (CMAQ model v5.1) for data assimilation of ground-level PM2.5, Geosci. Model Dev., 15, 2773-2790, 10.5194/gmd-15-2773-2022, 2022.
Peng, X., Xiao, F., Ohfuchi, W., and Fuchigami, H.: Conservative Semi-Lagrangian Transport on a Sphere and the Impact on Vapor Advection in an Atmospheric General Circulation Model, Monthly Weather Review, 133, 504-520, 10.1175/mwr-2869.1, 2005.
Peng, Y., Wang, H., Hou, M., Jiang, T., Zhang, M., Zhao, T., and Che, H.: Improved method of visibility parameterization focusing on high humidity and aerosol concentrations during fog–haze events: Application in the GRAPES_CAUCE model in Jing-Jin-Ji, China, Atmospheric Environment, 222, 117139, 10.1016/j.atmosenv.2019.117139, 2020.
Peng, Y., Wang, H., Zhang, X., Zhao, T., Jiang, T., Che, H., Zhang, X., Zhang, W., and Liu, Z.: Impacts of PBL schemes on PM2.5 simulation and their responses to aerosol-radiation feedback in GRAPES_CUACE model during severe haze episodes in Jing-Jin-Ji, China, Atmospheric Research, 248, 10.1016/j.atmosres.2020.105268, 2021.
Peng, Z., Liu, Z., Chen, D., and Ban, J.: Improving PM2. 5 forecast over China by the joint adjustment of initial conditions and source emissions with an ensemble Kalman filter, Atmos. Chem. Phys., 17, 4837-4855, 10.5194/acp-17-4837-2017, 2017.
Skachko, S., Ménard, R., Errera, Q., Christophe, Y., and Chabrillat, S.: EnKF and 4D-Var data assimilation with chemical transport model BASCOE (version 05.06), Geoscientific Model Development, 9, 2893-2908, 10.5194/gmd-9-2893-2016, 2016.
Sokhi, R. S., Moussiopoulos, N., Baklanov, A., Bartzis, J., Coll, I., Finardi, S., Friedrich, R., Geels, C., Grönholm, T., Halenka, T., Ketzel, M., Maragkidou, A., Matthias, V., Moldanova, J., Ntziachristos, L., Schäfer, K., Suppan, P., Tsegas, G., Carmichael, G., Franco, V., Hanna, S., Jalkanen, J.-P., Velders, G. J. M., and Kukkonen, J.: Advances in air quality research – current and emerging challenges, Atmos. Chem. Phys., 22, 4615-4703, 10.5194/acp-22-4615-2022, 2022.
Tang, X., Zhu, J., Wang, Z. F., and Gbaguidi, A.: Improvement of ozone forecast over Beijing based on ensemble Kalman filter with simultaneous adjustment of initial conditions and emissions, Atmos. Chem. Phys., 11, 12901-12916, 10.5194/acp-11-12901-2011, 2011.
Tang, Y., Chai, T., Pan, L., Lee, P., Tong, D., Kim, H.-C., and Chen, W.: Using optimal interpolation to assimilate surface measurements and satellite AOD for ozone and PM2.5: A case study for July 2011, Journal of the Air & Waste Management Association, 65, 1206-1216, 10.1080/10962247.2015.1062439, 2015.
Ting, Y.-C., Young, L.-H., Lin, T.-H., Tsay, S.-C., Chang, K.-E., and Hsiao, T.-C.: Quantifying the impacts of PM2.5 constituents and relative humidity on visibility impairment in a suburban area of eastern Asia using long-term in-situ measurements, Science of The Total Environment, 818, 151759, 10.1016/j.scitotenv.2021.151759, 2022.
Wang, C., An, X., Hou, Q., Sun, Z., Li, Y., and Li, J.: Development of four-dimensional variational assimilation system based on the GRAPES–CUACE adjoint model (GRAPES–CUACE-4D-Var V1.0) and its application in emission inversion, Geosci. Model Dev., 14, 337-350, 10.5194/gmd-14-337-2021, 2021.
Wang, D., You, W., Zang, Z., Pan, X., He, H., and Liang, Y.: A three-dimensional variational data assimilation system for a size-resolved aerosol model: Implementation and application for particulate matter and gaseous pollutant forecasts across China, Science China Earth Sciences, 63, 1366-1380, 10.1007/s11430-019-9601-4, 2020.
Wang, H. and Niu, T.: Sensitivity studies of aerosol data assimilation and direct radiative feedbacks in modeling dust aerosols, Atmospheric Environment, 64, 208-218, 10.1016/j.atmosenv.2012.09.066, 2013.

Wang, H., Gong, S., Zhang, H., Chen, Y., Shen, X., Chen, D., Xue, J., Shen, Y., Wu, X., and Jin, Z.: A new-generation sand and dust storm forecasting system GRAPES_CUACE/Dust: Model development, verification and numerical simulation, Chinese Science Bulletin, 55, 635-649, 10.1007/s11434-009-0481-z, 2010a.

Wang, H., Zhang, X., Gong, S., Chen, Y., Shi, G., and Li, W.: Radiative feedback of dust aerosols on the East Asian dust storms, Journal of Geophysical Research: Atmospheres, 115, 10.1029/2009JD013430, 2010b.

Wang, H., Peng, Y., Zhang, X., Liu, H., Zhang, M., Che, H., Cheng, Y., and Zheng, Y.: Contributions to the explosive growth of PM2.5 mass due to aerosol–radiation feedback and decrease in turbulent diffusion during a red alert heavy haze in Beijing–Tianjin–Hebei, China, Atmos. Chem. Phys., 18, 17717-17733, 10.5194/acp-18-17717-2018, 2018.

Wang, H., Xue, M., Zhang, X. Y., Liu, H. L., Zhou, C. H., Tan, S. C., Che, H. Z., Chen, B., and Li, T.: Mesoscale modeling study of the interactions between aerosols and PBL meteorology during a haze episode in Jing-Jin-Ji (China) and its nearby surrounding region - Part 1: Aerosol distributions and meteorological features, Atmospheric Chemistry & Physics, 15, 3257, 10.5194/acp-15-3257-2015, 2015a.

Wang, H., Shi, G. Y., Zhang, X. Y., Gong, S. L., Tan, S. C., Chen, B., et al.: Mesoscale modelling study of the interactions between aerosols and PBL meteorology during a haze episode in China Jing–Jin–Ji and its near surrounding region – Part 2: Aerosols' radiative feedback effects. Atmos. Chem. Phys., 15(6), 3277-3287. 10.5194/acp-15-3277-2015, 2015b

Wang, P., Wang, H., Wang, Y. Q., Zhang, X. Y., Gong, S. L., Xue, M., Zhou, C. H., Liu, H. L., An, X. Q., Niu, T., and Cheng, Y. L.: Inverse modeling of black carbon emissions over China using ensemble data assimilation, Atmospheric Chemistry and Physics, 16, 989-1002, 10.5194/acp-16-989-2016, 2016.

Wang, Y. Q., Zhang, X. Y., Gong, S. L., Zhou, C. H., Hu, X. Q., Liu, H. L., Niu, T., and Yang, Y. Q.: Surface observation of sand and dust storm in East Asia and its application in CUACE/Dust, Atmos. Chem. Phys., 8, 545-553, 10.5194/acp-8-545-2008, 2008.

Xie, J. and Zhu, J.: Ensemble optimal interpolation schemes for assimilating Argo profiles into a hybrid coordinate ocean model, Ocean Modelling, 33, 283-298, 10.1016/j.ocemod.2010.03.002, 2010.

Ye, H., Pan, X., You, W., Zhu, X., Zang, Z., Wang, D., Zhang, X., Hu, Y., and Jin, S.: Impact of CALIPSO profile data assimilation on 3-D aerosol improvement in a size-resolved aerosol model, Atmospheric Research, 264, 105877, 10.1016/j.atmosres.2021.105877, 2021.

Yu, X., Ma, J., An, J., Yuan, L., Zhu, B., Liu, D., Wang, J., Yang, Y., and Cui, H.: Impacts of meteorological condition and aerosol chemical compositions on visibility impairment in Nanjing, China, Journal of Cleaner Production, 131, 112-120, 10.1016/j.jclepro.2016.05.067, 2016.

Zhai, S., An, X., Zhao, T., Sun, Z., Wang, W., Hou, Q., Guo, Z., and Wang, C.: Detection of critical PM2.5 emission sources and their contributions to a heavy haze episode in Beijing, China, using an adjoint model, Atmos. Chem. Phys., 18, 6241-6258, 10.5194/acp-18-6241-2018, 2018.

Zhang J.P., Hu J.T., Wang X.M.: Preliminary application of ensemble optimal interpolation data assimilation method on air quality numerical modeling in the Pearl River Delta, Acta Scientiae Circumstantiae,34(3): 558-566, DOI: 10.13671/j.hjkxxb.2014.0103, 2014.Zhang, F., Zhang, M., Huang, X.-Y., and Zhang, X.: Intercomparison of an Ensemble Kalman Filter with Three- and Four-Dimensional Variational Data Assimilation Methods in a Limited-Area Model over the Month of June 2003, Monthly Weather Review, 139, 566-572, 10.1175/2010mwr3610.1, 2011.

Zhang, L., Shao, J., Lu, X., Zhao, Y., Hu, Y., Henze, D. K., Liao, H., Gong, S., and Zhang, Q.: Sources and Processes Affecting Fine Particulate Matter Pollution over North China: An Adjoint Analysis of the Beijing APEC Period, Environ Sci Technol, 50, 8731-8740, 10.1021/acs.est.6b03010, 2016.

Zhang, S., Tian, X., Zhang, H., Han, X., and Zhang, M.: A nonlinear least squares four-dimensional variational data assimilation system for PM2.5 forecasts (NASM): Description and preliminary evaluation, Atmospheric Pollution Research, 12, 122-132, 10.1016/j.apr.2021.03.003, 2021.

Zhang, W., Zhang, X., and Wang, H.: The Role of Aerosol-Radiation Interaction in the Meteorology Prediction at the Weather Scale in the Numerical Weather Prediction Model, Geophysical Research Letters, 49, e2021GL097026, 10.1029/2021GL097026, 2022.

Zheng, B., Zhang, Q., Zhang, Y., He, K. B., Wang, K., Zheng, G. J., Duan, F. K., Ma, Y. L., and Kimoto, T.: Heterogeneous chemistry: a mechanism missing in current models to explain secondary inorganic aerosol formation during the January 2013 haze episode in North China, Atmospheric Chemistry and Physics, 15, 2031-2049, 10.5194/acp-15-2031-2015, 2015.

Zheng, H., Liu, J., Tang, X., Wang, Z., Wu, H., Yan, P., and Wang, W.: Improvement of the Real-time PM2.5 Forecast over the Beijing-Tianjin-Hebei Region using an Optimal Interpolation Data Assimilation Method, Aerosol and Air Quality Research, 18, 1305-1316, 10.4209/aaqr.2017.11.0522, 2018.

Zhou, C.-H., Gong, S., Zhang, X.-Y., Liu, H.-L., Xue, M., Cao, G.-L., An, X.-Q., Che, H.-Z., Zhang, Y.-M., and Niu, T.: Towards the improvements of simulating the chemical and optical properties of Chinese aerosols using an online coupled model – CUACE/Aero, Tellus B: Chemical and Physical Meteorology, 64, 18965, 10.3402/tellusb.v64i0.18965, 2012.

Zhu Jiang, Tang Xiao, Wang Zifa, et al.: A review of air quality data assimilation methods and their application [J]. Chinese Journal of Atmospheric Sciences (in Chinese), 42 (3): 607−620, 10.3878/j. issn.1006-9895.1802.17260, 2018.

Table1. Mass concentration limit of $PM_{2.5}$ and its corresponding air quality level and air pollution index (API)

$PM_{2.5}$ concentration limit (ug m^{-3})	Air quality description	level	API
35	excellent	I	0-50
75	good	II	51-100
115	light pollution	III	101-150
150	moderate pollution	IV	151-200
250	heavy pollution	V	201-300
>250	hazardous pollution	VI	>300

Table2. Experimental design.

Name	Experiment	Design
Control experiment	CR00	Model control run without DA begin at 0000 UTC every day and forecast 24 hours
	CR12	Model control run without DA begin at 1200 UTC every day and forecast 24 hours
Sensitivity experiment	Lxxkm-N48	assimilation at 0000 UTC with fixed ensemble size N of 48 and different localization length-scale Lxx of 20, 40, 60, 80, 100 km
	L80km-Nyy	assimilation at 0000 UTC with fixed localization length-scale L of 80 km and different ensemble size Nyy of 24, 48, 72, 96, 120, 144
Cycling assimilation experiment	DA00	Model forecast with assimilation at 0000 UTC every day
	DA12	Model forecast with assimilation at 1200 UTC every day
	DA00&12	Model forecast with assimilation at 0000 UTC and 1200UTC everyday

Table3. Statistics of $PM_{2.5}$ concentrations for verifications sites of the initial field without (CR) and with assimilation at 0000 UTC each day from 1 to 31 December 2016. Assimilation sensitivity experiments were performed with 48 ensemble samples and length-scale L of 20, 40, 60, 80, 100km respectively and only assimilated the assimilation sites.

	CORR	RMSE (μg m^{-3})	MB (μg m^{-3})	ME (μg m^{-3})
CR	0.56	60.1	8.5	41.7
20	0.77	48.2	4.1	30.2
40	0.82	41.6	3.2	25.9
60	0.81	43.1	3.5	26.8
80	0.80	44.9	3.8	27.0
100	0.79	46.0	4.0	28.2

660 **Table4. Statistics of $PM_{2.5}$ concentrations for verifications sites of the initial field withthout (CR) and with assimilation at 0000 UTC each day from 1 to 31 December 2016. Assimilation sensitivity experiments were performed with a localization length-scale L of 80 km and an ensemble size of 24, 48, 72, 96, 120, and 144, respectively and only assimilated the assimilation sites.**

	CORR	RMSE (μg m^{-3})	MB (μg m^{-3})	ME (μg m^{-3})
CR	0.56	60.1	8.5	41.7
24	0.76	48.6	4.2	30.8
48	0.80	44.9	3.8	27.0
72	0.81	42.4	3.4	25.9
96	0.82	40.7	2.9	25.7
120	0.80	44.1	3.6	26.2
144	0.79	45.8	3.9	27.3

Table5. Statistics of initial $PM_{2.5}$ concentrations for assimilation sites (DA) and verifications sites (Ve) before EnOI (BF) and after EnOI (AF) at 0000 UTC on 16, 19, 20 and 23 December 2016, respectively.

Date	site	IC	CORR	RMSE ($\mu g\ m^{-3}$)	ME ($\mu g\ m^{-3}$)	MB ($\mu g\ m^{-3}$)
16	DA	BF	0.50	50.8	9.1	38.2
		AF	0.98	11.0	0.9	7.1
	Ve	BF	0.48	56.5	9.7	42.8
		AF	0.73	39.1	2.5	25.2
19	Da	BF	0.65	81.5	-9.3	55.2
		AF	0.98	17.3	-1.2	10.4
	Ve	BF	0.66	79.2	-5.7	50.2
		AF	0.85	56.1	1.3	32.4
20	DA	BF	0.67	95.0	-24.2	64.5
		AF	0.99	19.1	-2.7	10.2
	Ve	BF	0.66	94.7	-20.5	60.5
		AF	0.87	60.2	-5.1	35.1
23	DA	BF	0.52	47.6	20.6	36.9
		AF	0.97	10.8	2.1	6.8
	Ve	BF	0.50	50.3	23.3	37.9
		AF	0.75	31.4	6.0	20.6

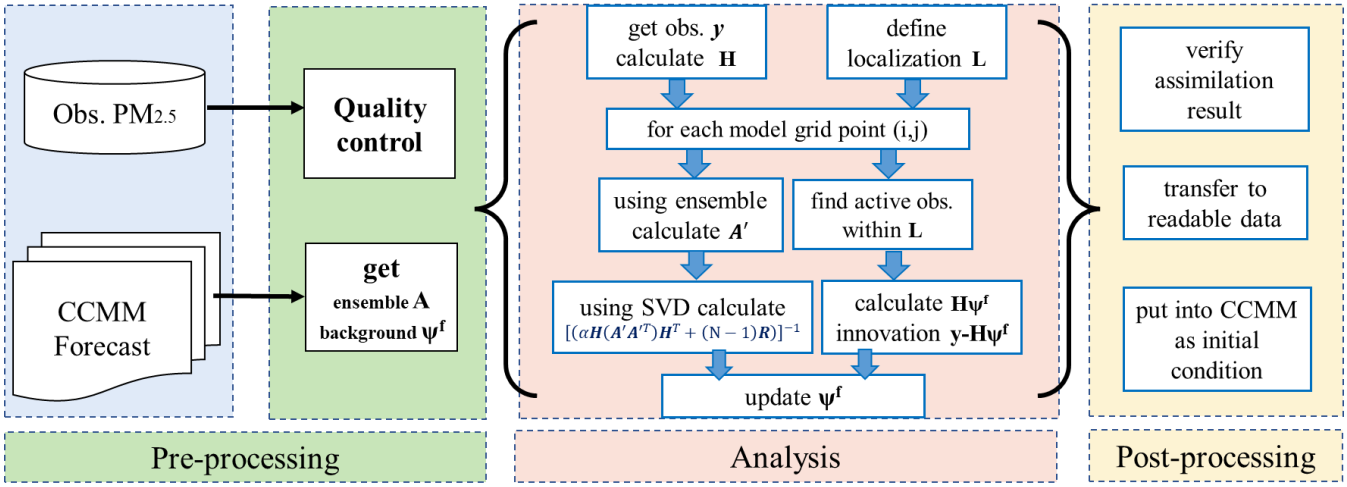

Figure 1. Flow chart of the main procedures for EnOI initial field assimilation system. The Obs. $PM_{2.5}$ is ground-based observation of $PM_{2.5}$. The CCMM is coupled chemistry meteorology models. SVD is singular value decomposition

675

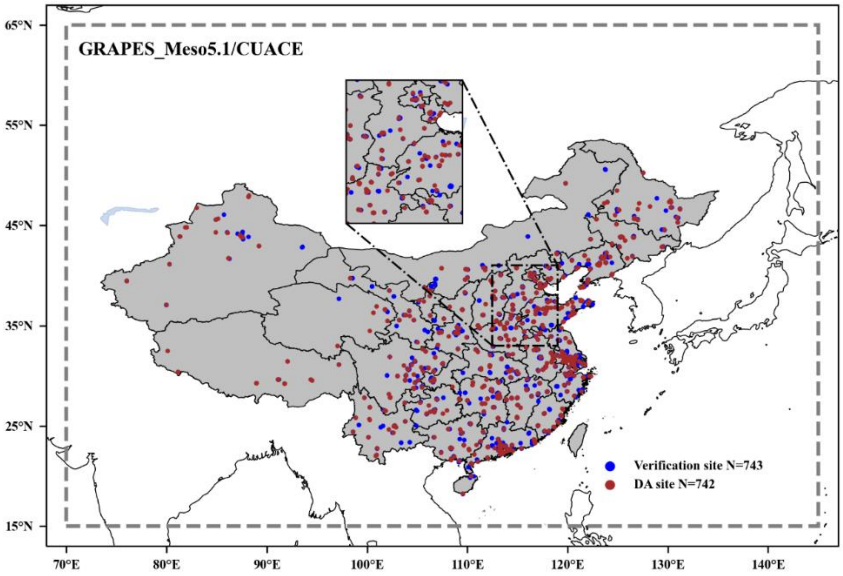

Figure 2. Simulation domain of GRAPES_Meso5.1/CUACE. Minor region represents North China (NC). The locations of ground stations in China mainland are marked on the maps with blue and brown dots. The blue and brown dots represent verification sites and assimilation sites, respectively. "N=743" means there are 743 verification sites. "N=742" means there are 742 DA sites.

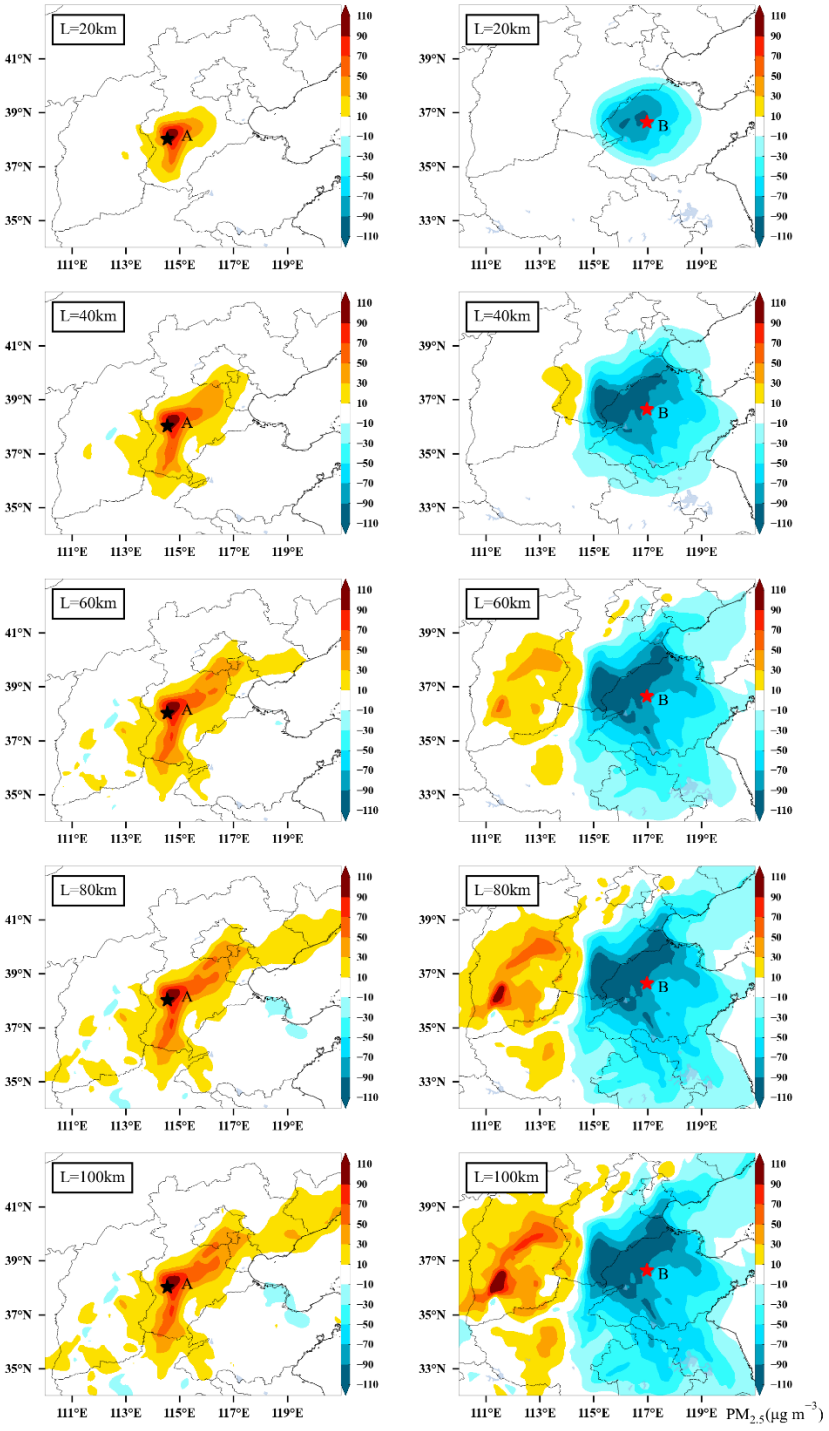

Figure 3. Spatial distribution of $PM_{2.5}$ analysis increments after assimilation of initial fields at 0000 UTC on 15 December 2016, for assimilation site A (38.0° N, 114.5° E) only (left column) and assimilation site B (36.6° N, 116.9° E) only (right column) with fixed ensemble size 48 and different localization length-scale of 20, 40, 60, 80, 100km.

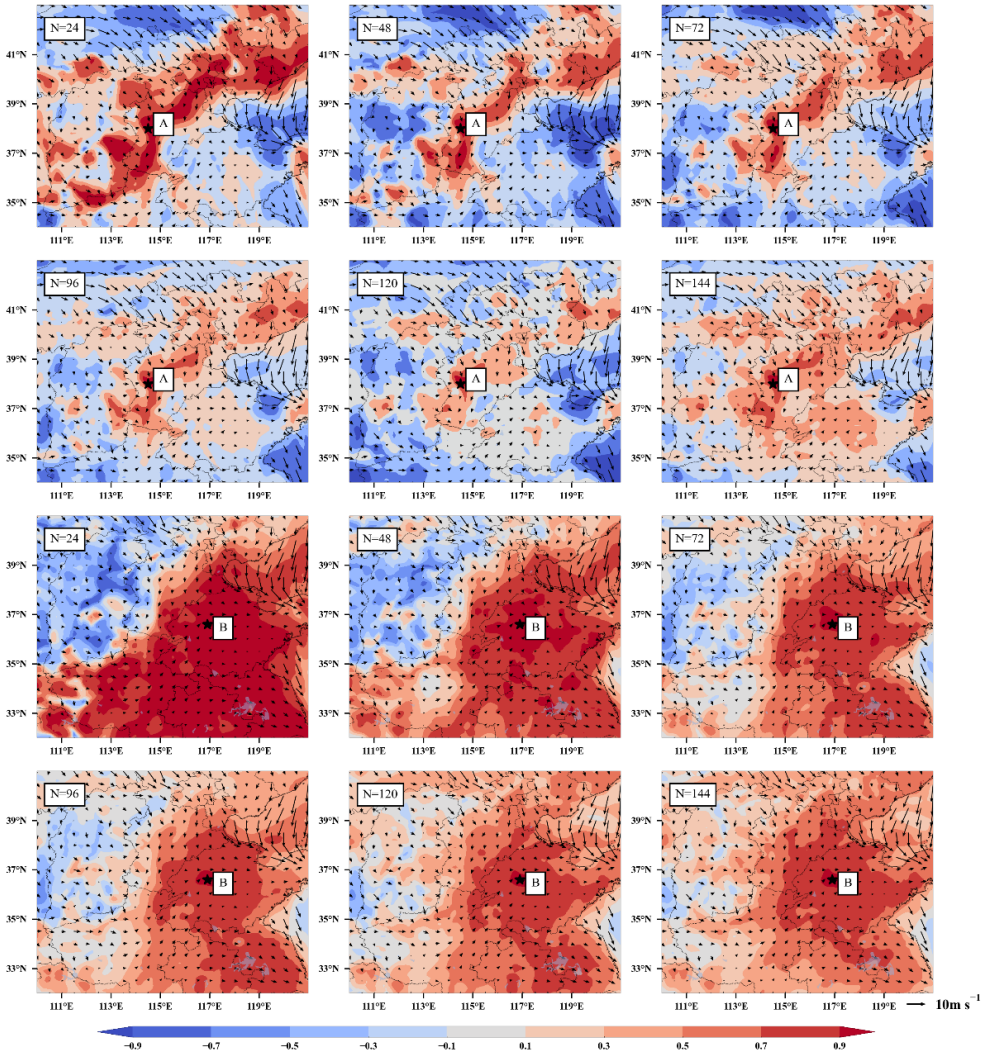

Figure 4. Spatial distribution of correlation coefficients of background error for site A (38.0° N, 114.5° E) (rows 1, 2) and site B (36.6° N, 116.9° E) (rows 3, 4) with different ensemble size N of 24, 48, 72, 96, 120, 144 and wind vectors at 0000 UTC on 15 December 2016.

690

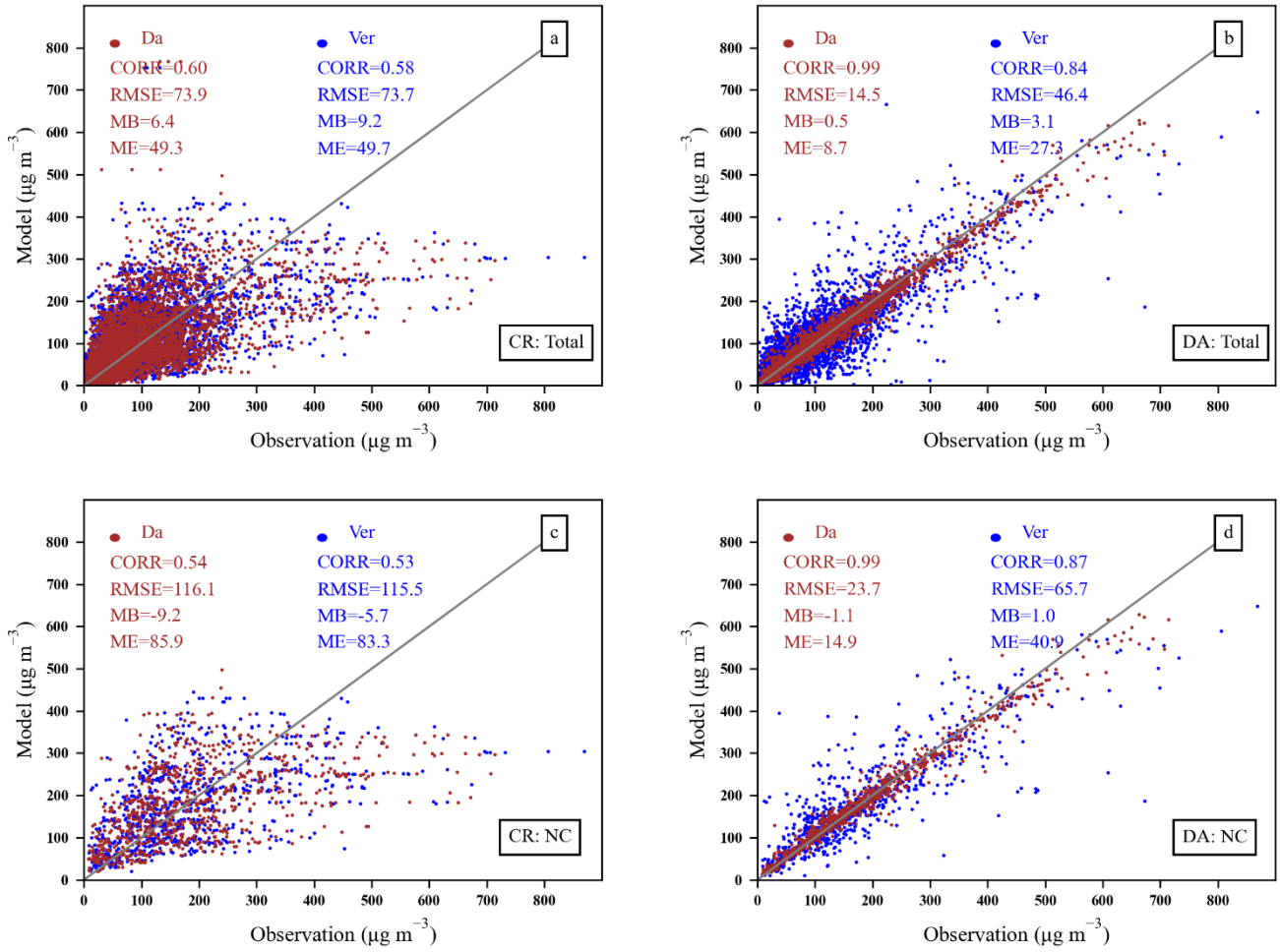

Figure 5. Scatter plot of $PM_{2.5}$ concentrations from the control experiment (a,c) and the assimilation experiment (b, d). The ensemble size in the assimilation experiment is 96 and the length-scale L is 40 km. Brown (Da) and blue (Ver) dots are assimilation sites and validation sites respectively. a, b is for mainland China (Total), c, d is for North China (NC).

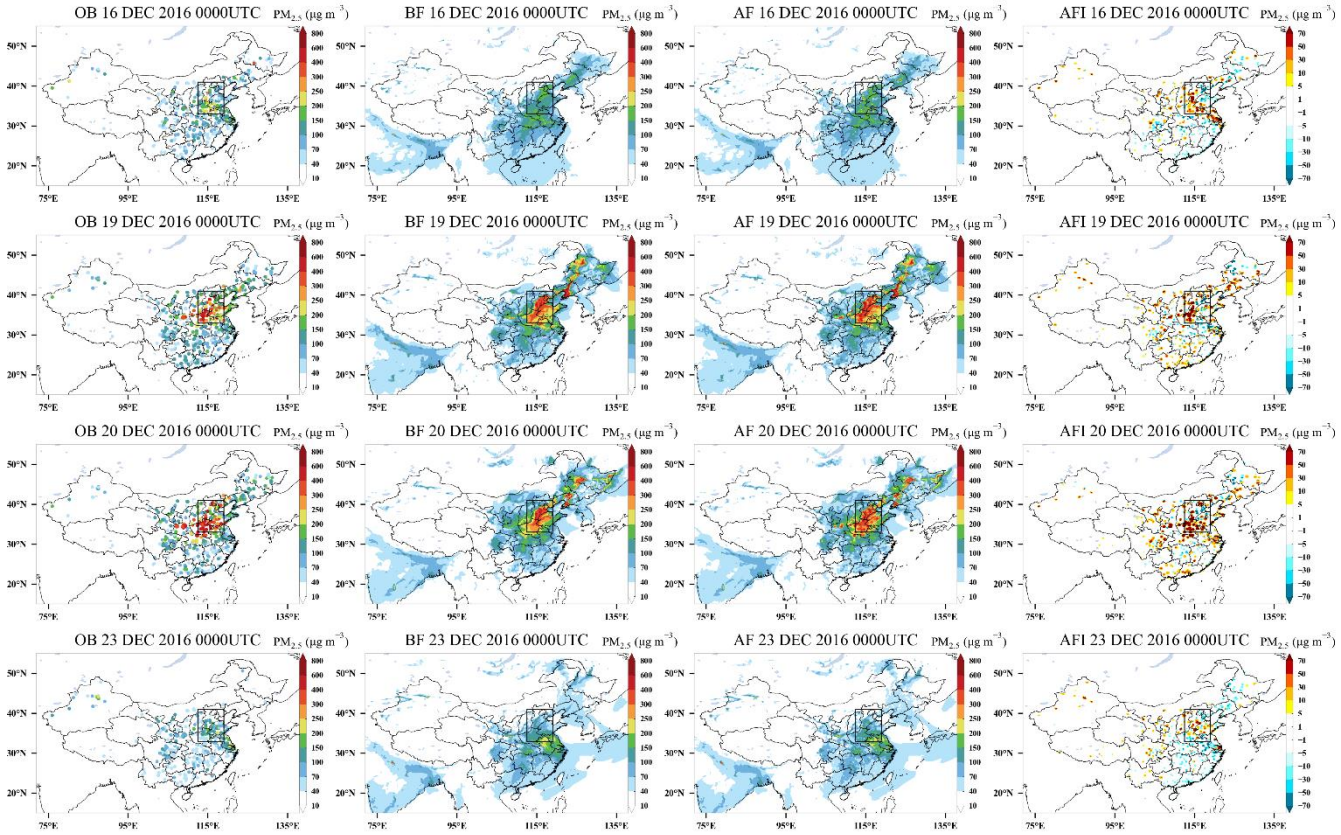

Figure 6. Snapshots of the horizontal distributions of $PM_{2.5}$ observation (OB), before (BF) and after (AF) the application of EnOI technique, analysis field increment (AFI) at 0000 UTC on 16, 19, 20, and 23, December 2016. The black box area, representing North China (NC).

705

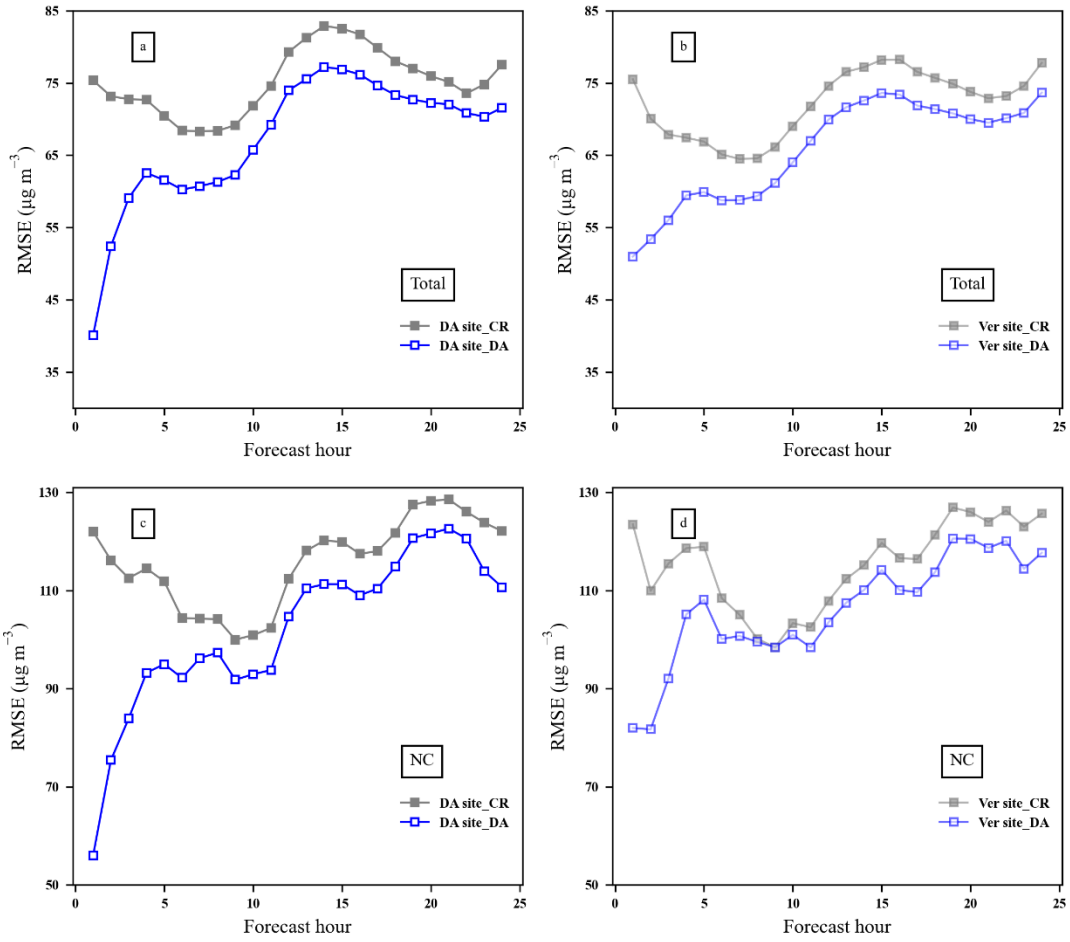

Figure 7. The average RMSE value of surface $PM_{2.5}$ forecasts as a function of forecast time over (a) China Mainland for DA sites, (b) China Mainland for verification sites, (c) North China for DA sites, (d) North China for verification site.

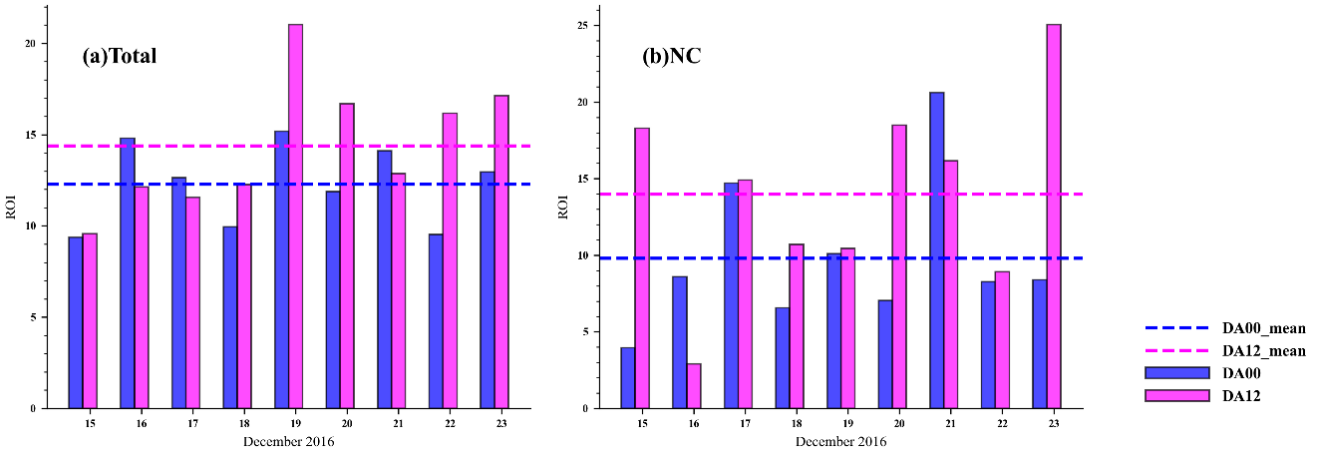

Figure 8. Rate of improvement (ROI, unit: %) by data assimilation in 1d (24h) predictions for 15 to 23 December 2016 over Mainland China (a), North China (b). The ROI is the ratio of the reduced RMSE statistical metrics to those for the CR simulation. DA00 and DA12 represent the initial field assimilation using EnOI at 0000 UTC and 1200 UTC each day, respectively. DA00_mean and DA12_mean represent the mean ROI over 15 to 23 December 2016 of DA00 and DA12, respectively.

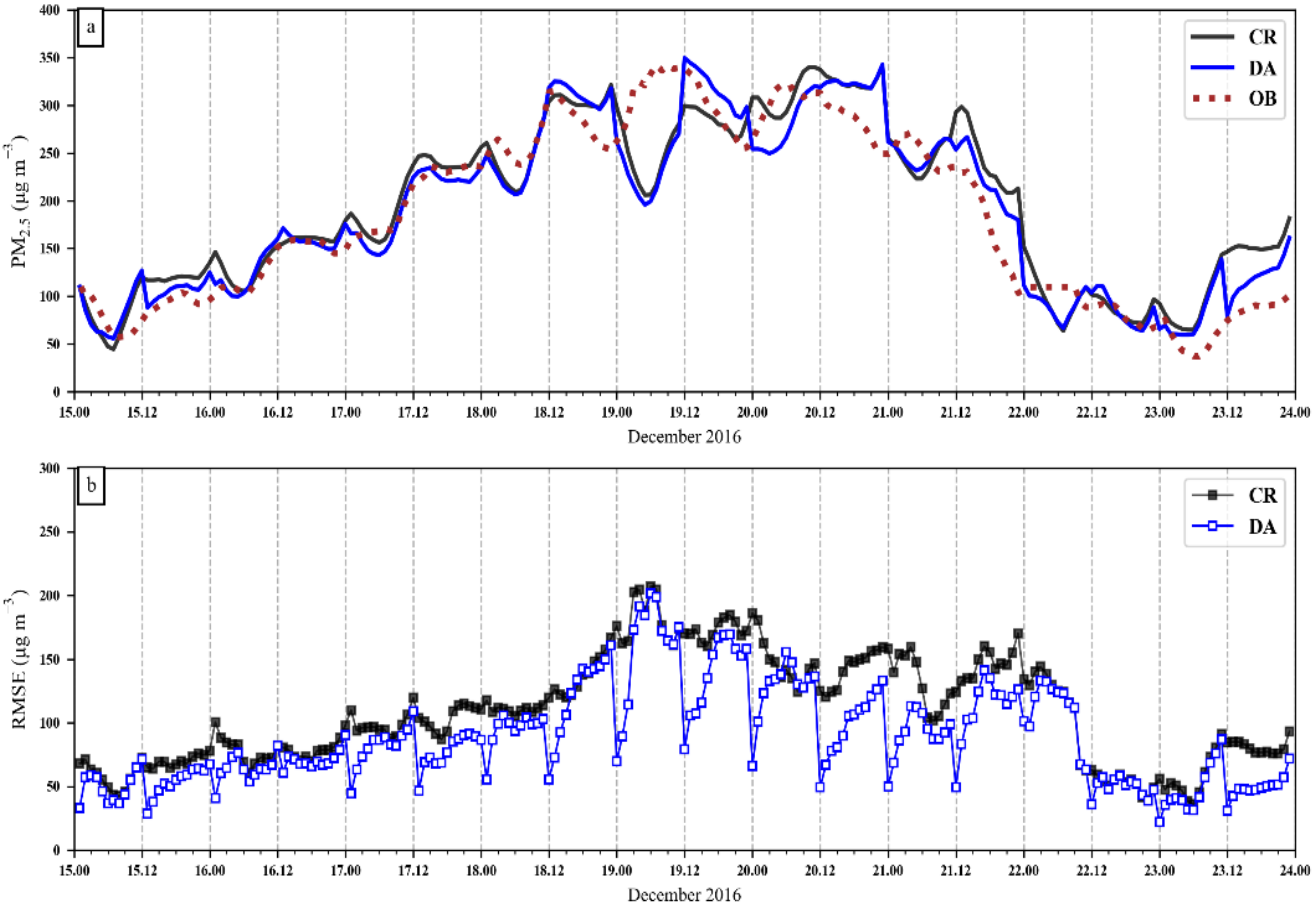

Figure 9. Time series of hourly $PM_{2.5}$ concentration (a) and RMSE between forecasts and observations (b) from 15 December to 23 December 2016 in North China. Red dots: observations, black line: forecasts from control experiment (CR), blue line: forecasts from experiment with initial field assimilation at 0000UTC and 1200UTC (DA), black line with dots: RMSE between CR forecasts and observations, blue line with dots: RMSE between CR forecasts and observations. The values are averages calculated against all the observation sites in North China.

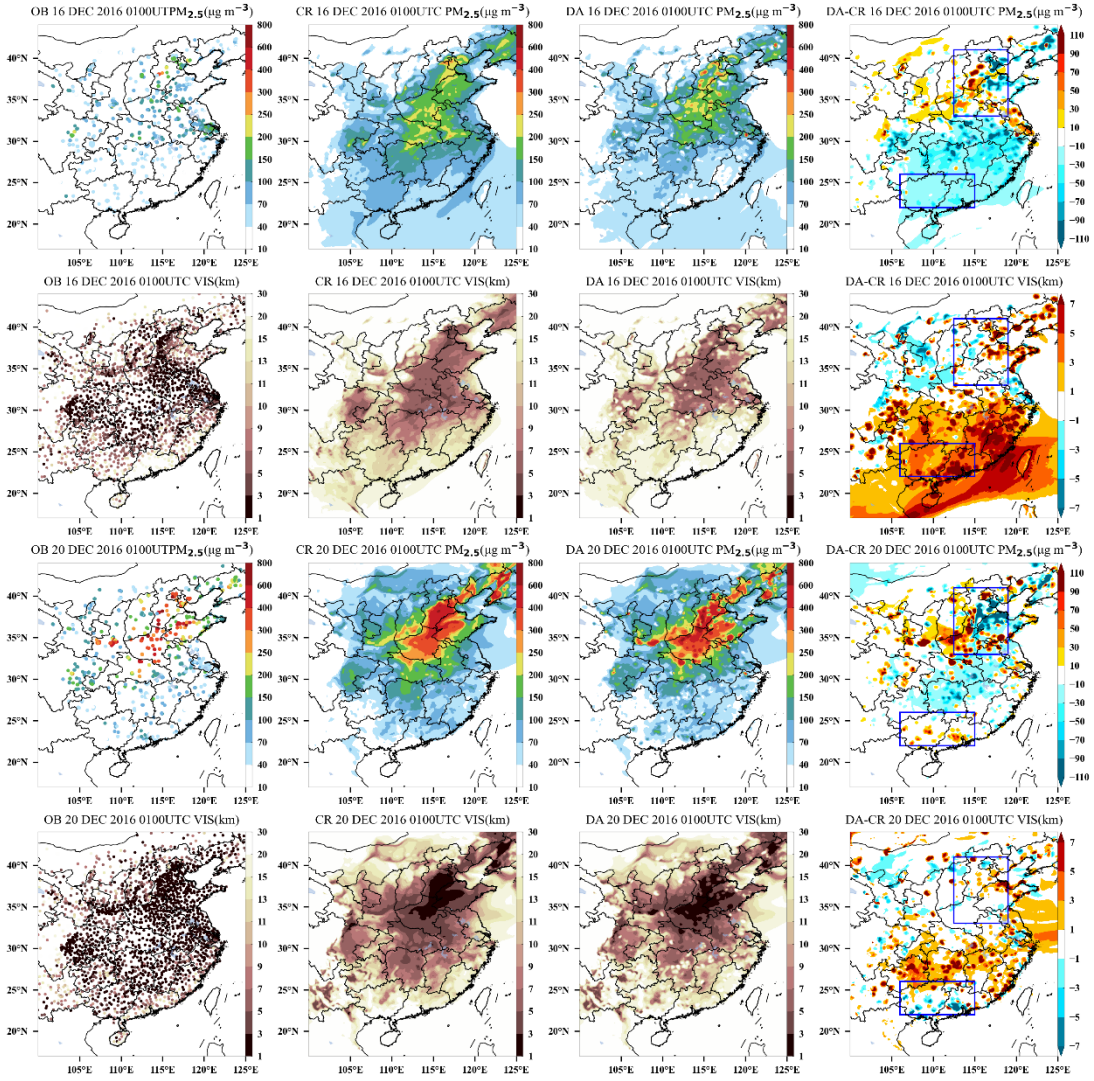

Figure 10. Snapshots of $PM_{2.5}$ and visibility horizontal distribution for control (CR), assimilation (DA), observation (OB), and increment (DA-CR) at 0100 UTC after assimilation of the initial field at 0000 UTC on 16 and 20 December 2016.The upper box represents North China and the lower box represents Guangxi and Hainan in China.

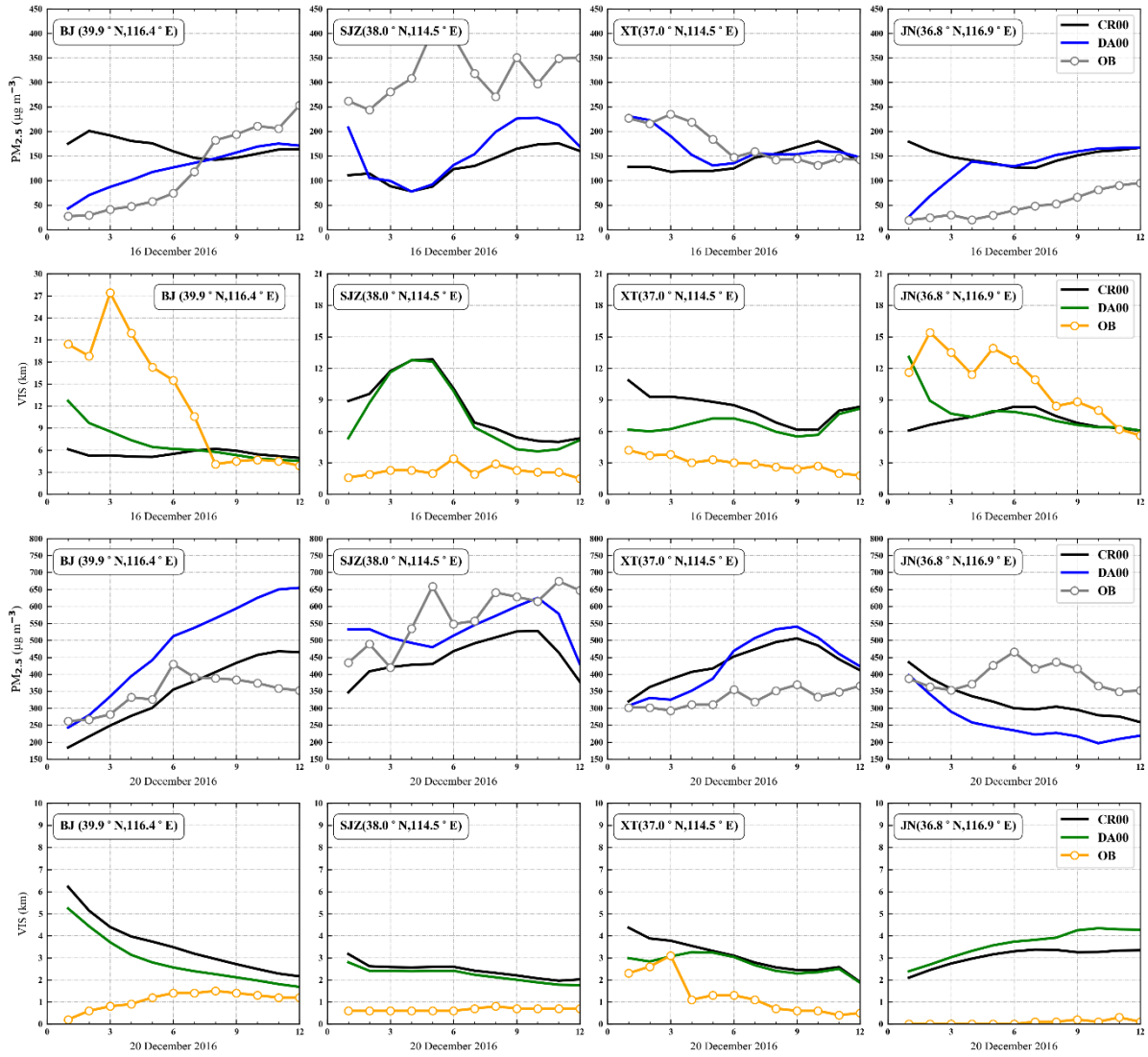

730 **Figure 11. Comparison between $PM_{2.5}$ and visibility observations and model forecast at four cities without (CR00) and with assimilation (DA00) of the initial field at 0000 UTC on 16 and 20 December 2016. Four cities are exemplified, from left to right, Beijing (BJ), Shijiazhuang (SJZ), Xingtai (XT), Jinan (JN). The labels on the x-axis refer to the first 12 forecast hours of the day. $PM_{2.5}$ observations: grey line with circles, visibility observations: orange line with circles, $PM_{2.5}$ and visibility model forecast without assimilation: black line, $PM_{2.5}$ model forecast with assimilation: blue line, visibility model forecast with assimilation: green line.**